

A NOVEL NUMERICAL METHOD FOR THE SEMICLASSICAL LIMIT OF THE SCHRÖDINGER EQUATION AND THE VLASOV-POISSON EQUATIONS

SHI JIN AND DONGMING WEI

ABSTRACT. We propose a novel numerical method for the semiclassical limit of the Schrödinger equation. When using deterministic particle methods, point values of the computed solutions have to be recovered from their singular particle approximations by using some smoothing procedure. The choice of the smoothing procedure is rather flexible. Moreover, there is always a parameter associated with the smoothing procedure: if this parameter is too large, the numerical solution loses its accuracy; if it is too small, oscillation appears. No explicit formula has been given on how to choose this parameter.

Based on the idea of [30], we develop a particle method in which we use the *conservation of charge* for the reconstruction of density. This method avoids the recovery step of the previous particle methods, thus it is simpler and more accurate. In particular it gives more accurate field quantities. Consequently, we apply the new method to the Vlasov-Poisson equations, which yields more accurate density and electric field in each time step. We carry out numerical experiments in both one and two dimensions for the Schrödinger equation and Vlasov-Poisson equations to verify the method. Some comparisons with the other particle methods are also made.

1. INTRODUCTION

In this paper, we propose a novel numerical method for the Liouville equation

$$f_t + H_{\xi} \cdot \nabla_{\mathbf{x}} f - H_{\mathbf{x}} \cdot \nabla_{\xi} f = 0, \quad t > 0, \quad \mathbf{x}, \xi \in \mathbb{R}^d, \quad (1.1)$$

with initial data

$$f(0, \mathbf{x}, \xi) = \rho_0(\mathbf{x})\delta(\xi - \mathbf{u}_0(\mathbf{x})). \quad (1.2)$$

The function $f(t, \mathbf{x}, \xi)$ is the density distribution of particles depending on position \mathbf{x} , time t and velocity ξ . The solution to this problem is a superposition of delta functions of variable weight concentrating on the bi-characteristic strips of the equation which is governed by the Hamiltonian system

$$\frac{\partial \mathbf{x}}{\partial t} = \nabla_{\xi} H, \quad \frac{\partial \xi}{\partial t} = -\nabla_{\mathbf{x}} H,$$

with the Hamiltonian

$$H(\mathbf{x}, \xi) = \frac{1}{2}|\xi|^2 + V(\mathbf{x}), \quad (1.3)$$

where $V(\mathbf{x})$ is the potential function.

Date: January 2, 2011.

Acknowledgment. This work was partially supported by NSF grant No. DMS-0608720, and NSF FRG grant DMS-0757285. SJ was also supported by a Van Vleck Distinguished Research Prize and a Vilas Associate Award from University of Wisconsin-Madison.

We will also consider the Vlasov-Poisson equations which are just (1.1) with potential V given by

$$\Delta_{\mathbf{x}}V = \int_{\mathbb{R}^d} f(\mathbf{x}, \mathbf{v}, t) d\mathbf{v} =: \rho(\mathbf{x}, t). \quad (1.4)$$

Equation (1.1) provides a phase space description of the semiclassical limit of the Schrödinger equation [9, 19]:

$$i\hbar\partial_t\psi^h = -\frac{\hbar^2}{2}\Delta\psi^h + V(\mathbf{x})\psi^h, \quad \mathbf{x} \in \mathbb{R}^d, \quad (1.5)$$

where ψ^h is the complex-valued wave function, \hbar the reduced Planck constant. In this setting, one typically considers the Schrödinger equation (1.5) with the WKB initial data of the form

$$\psi(\mathbf{x}, 0) = A_0(\mathbf{x}) \exp(iS_0(\mathbf{x})/\hbar) \quad (1.6)$$

with smooth S_0 . In the semiclassical limit $\hbar \rightarrow 0$, the Wigner transform of ψ is f that satisfies the Liouville equation (1.1) with the mono-kinetic initial data (1.2):

$$f(0, \mathbf{x}, \boldsymbol{\xi}) = |A_0(\mathbf{x})|^2 \delta(\boldsymbol{\xi} - \nabla_{\mathbf{x}}S_0(\mathbf{x})) =: \rho_0(\mathbf{x})\delta(\boldsymbol{\xi} - \nabla_{\mathbf{x}}S_0(\mathbf{x})). \quad (1.7)$$

The Vlasov-Poisson equations arise in semiconductor device modeling [23] and plasma physics [18]. For mathematical analysis of this system see [2, 20, 31, 21, 22], while for numerical methods see [11, 1, 8, 28, 29].

When one closes (1.1) and (1.2) with the moments—which give the density and momentum of particles—the moment system satisfies the pressureless gas dynamics equations, which develop delta-shock solutions in finite time, corresponding to caustics in geometric optics. Beyond the caustics, only the multi-valued solutions are physically relevant [27, 12]. The computation of multivalued solutions in geometrical optics and semiclassical limit of the Schrödinger equation, using the Liouville equation (1.1) in the Eulerian level set framework, has been an active area of research in recent years, see for examples [24, 3, 17, 14]. Recent overviews of this subject can be found in [7, 13].

We focus our attention on the Lagrangian particle methods. When using the particle method, one has to recover the point values of the computational solutions from their singular particle approximations which are Dirac delta functions. The most common approach is to approximate the Dirac delta function by its convolution with a smooth kernel, see, e.g., [5, 26, 6]. For a comparison between the convolution recovery and other redistribution recovery strategies, see [4]. In this paper, we propose a more accurate recovery strategy. The idea was first introduced in [30] to deal with the 1D Vlasov-Poisson equations with electron sheet initial data, and it is based on the following conservative quantity

$$\int_{\Upsilon(0)} f(0, \mathbf{x}, \boldsymbol{\xi}) d\boldsymbol{\xi} d\mathbf{x} = \int_{\Upsilon(t)} f(t, \mathbf{x}, \boldsymbol{\xi}) d\boldsymbol{\xi} d\mathbf{x}, \quad \forall \Upsilon(0) \subset \mathbb{R}^{2d}, \quad \forall t, \quad (1.8)$$

where

$$\Upsilon(t) = \left\{ (\mathbf{x}, \boldsymbol{\xi})(t, \mathbf{x}_0, \boldsymbol{\xi}_0) \left| \frac{d\mathbf{x}}{ds} = \boldsymbol{\xi}, \quad \frac{d\boldsymbol{\xi}}{ds} = -\nabla_{\mathbf{x}}V, \quad \mathbf{x}(0) = \mathbf{x}_0, \quad \boldsymbol{\xi}(0) = \boldsymbol{\xi}_0, \quad (\mathbf{x}_0, \boldsymbol{\xi}_0) \in \Upsilon(0) \right. \right\}.$$

We call this the *conservation of charge*. This allows one to get a more accurate density ρ , which is only a postprocessing for (1.1) of course, but for equations with a field, such as the Vlasov-Poisson equations (1.1) and (1.4), it provides a more accurate (time-dependent) potential—and

consequently the electric field $E = -\nabla_{\mathbf{x}}V$ at each time step, thus enhances the numerical accuracy overall in long time.

This paper is organized as follows. In section 2, we derive a formula of weak solutions of the Liouville equations with singular (measure-valued) initial data. In section 3, we describe a numerical density reconstruction method based on the conservation of charge (1.8) for one, two and general space dimensions. In section 4, we extend the method to the Vlasov-Poisson equations. In section 5, 1D and 2D numerical examples are given for the Liouville equations and Vlasov-Poisson equations, and comparisons are made with classical particle methods. This paper is concluded in section 6.

2. WEAK SOLUTION OF THE LIOUVILLE EQUATION WITH MEASURE-VALUED INITIAL DATA

We construct weak solutions of the one-dimensional Liouville equations with measure-valued initial data in section 2.1. Then we extend the result to the multi-dimensional case.

2.1. One space dimension.

First, we introduce the following definition which will be used in the weak solution formula.

Definition 2.1. Let C be a curve in the x - ξ space. Let $C(\alpha) = \{(x(\alpha), \xi(\alpha)) \mid \alpha \in \Omega\}$ be a parameterized form of C . The function $\vartheta_C(x, \xi)$ is a surface measure supported on the curve C , defined by

$$\int_{\mathbb{R}^2} \psi(x, \xi) \vartheta_C(x, \xi) d\xi dx = \int_{\Omega} \psi(x(\alpha), \xi(\alpha)) \left| \frac{dC(\alpha)}{d\alpha} \right| d\alpha, \quad \forall \psi \in C_0^\infty(\mathbb{R}^2), \quad (2.1)$$

where $\left| \frac{dC(\alpha)}{d\alpha} \right| = \sqrt{x'(\alpha)^2 + \xi'(\alpha)^2}$.

Remark 2.1. The definition 2.1 is independent of the choice of the parametrization α . Without loss of generality, we assume $\alpha \in \Omega = (a, b)$. Let $C(\beta) = \{(\tilde{x}(\beta), \tilde{\xi}(\beta)) \mid \beta \in (r, s)\}$ be another parameterized form of C . Then there exists a unique monotonic function g such that $(x(g(\beta)), \xi(g(\beta))) = (\tilde{x}(\beta), \tilde{\xi}(\beta))$. Therefore

$$\begin{aligned} & \int_a^b \psi(x(\alpha), \xi(\alpha)) \sqrt{x'(\alpha)^2 + \xi'(\alpha)^2} d\alpha \\ &= \int_{g^{-1}(a)}^{g^{-1}(b)} \psi(x(g(\beta)), \xi(g(\beta))) \sqrt{x'(g(\beta))^2 + \xi'(g(\beta))^2} d(g(\beta)) \\ &= \int_{g^{-1}(a)}^{g^{-1}(b)} \psi(\tilde{x}(\beta), \tilde{\xi}(\beta)) \sqrt{(\tilde{x}'(\beta)^2 + \tilde{\xi}'(\beta)^2) / g'(\beta)^2} g'(\beta) d\beta \\ &= \int_{g^{-1}(a)}^{g^{-1}(b)} \text{sign}(g'(\beta)) \psi(\tilde{x}(\beta), \tilde{\xi}(\beta)) \sqrt{(\tilde{x}'(\beta)^2 + \tilde{\xi}'(\beta)^2)} d\beta \\ &= \int_r^s \psi(\tilde{x}(\beta), \tilde{\xi}(\beta)) \sqrt{(\tilde{x}'(\beta)^2 + \tilde{\xi}'(\beta)^2)} d\beta. \end{aligned}$$

Remark 2.2. If one considers the mono-kinetic initial data then the following forms are equivalent in the weak sense:

$$f(0, x, \xi) = \rho_0(x)\delta(\xi - \nabla_x S_0(x)), \quad (2.2)$$

$$f(0, x, \xi) = \rho_0(x) \left| \frac{dC(x)}{dx} \right|^{-1} \vartheta_C, \quad (2.3)$$

where

$$C(x) = \left\{ (x, \xi(x)) = (x, \nabla_x S_0(x)) \mid x \in (-\infty, \infty) \right\}. \quad (2.4)$$

We verify it below: $\forall \psi \in C_0^\infty(\mathbb{R}^2)$,

$$\int_{-\infty}^{\infty} \int_{-\infty}^{\infty} \psi(x, \xi) \rho_0(x) \delta(\xi - \nabla_x S_0(x)) d\xi dx = \int_{-\infty}^{\infty} \psi(x, \nabla_x S_0(x)) \rho_0(x) dx, \quad (2.5)$$

$$\int_{-\infty}^{\infty} \int_{-\infty}^{\infty} \psi(x, \xi) \rho_0(x) \left| \frac{dC(x)}{dx} \right|^{-1} \vartheta_C d\xi dx = \int_{-\infty}^{\infty} \psi(x, \nabla_x S_0(x)) \rho_0(x) \left| \frac{dC(x)}{dx} \right|^{-1} \left| \frac{dC(x)}{dx} \right| dx. \quad (2.6)$$

Thus (2.5) and (2.6) are identical for all test functions, hence (2.2) and (2.3) are equivalent in the weak sense.

Remark 2.3. A general measure supported on the curve $C(\alpha)$ has the form $h(x, \xi) \vartheta_C$, such that

$$\int_{\mathbb{R}^2} \psi(x, \xi) h(x, \xi) \vartheta_C(x, \xi) d\xi dx = \int_{\Omega} \psi(x(\alpha), \xi(\alpha)) h(x(\alpha), \xi(\alpha)) \left| \frac{dC(\alpha)}{d\alpha} \right| d\alpha, \quad \forall \psi \in C_0^\infty(\mathbb{R}^2). \quad (2.7)$$

Notice that for function h , only the value on the curve C matters, that is, only

$$h(x(\alpha), \xi(\alpha)) =: h(\alpha) \quad (2.8)$$

matters. Therefore, we denote the measure as

$$h(x, \xi) \vartheta_C =: h(\alpha) \vartheta_{C(\alpha)}. \quad (2.9)$$

We give a formula for weak solutions of the 1D Liouville equations in the following theorem.

Theorem 2.1. Consider (1.1) subject to the delta function initial data, i.e., a measure supported on a curve $C(\alpha, 0) = \left\{ (x(\alpha, 0), \xi(\alpha, 0)) \mid \alpha \in \Omega \right\}$ which has the following form

$$f(0, x, \xi) = \varrho_0(\alpha) \left| \frac{dC(\alpha, 0)}{d\alpha} \right|^{-1} \vartheta_{C(\alpha, 0)}. \quad (2.10)$$

Denote the solution of the initial value problem of the Hamiltonian system

$$\frac{dx}{dt} = \xi, \quad \frac{d\xi}{dt} = -\nabla_x V, \quad x(0) = x(\alpha, 0), \quad \xi(0) = \xi(\alpha, 0), \quad (2.11)$$

by $(x(\alpha, t), \xi(\alpha, t))$. Then

$$f(t, x, \xi) = \varrho_0(\alpha) \left| \frac{dC(\alpha, t)}{d\alpha} \right|^{-1} \vartheta_{C(\alpha, t)} \quad (2.12)$$

is a weak solution to (1.1), which is a delta function supported on the curve

$$C(\alpha, t) = \left\{ (x(\alpha, t), \xi(\alpha, t)) \mid \alpha \in \Omega \right\}.$$

Moreover, for every interval (β, γ) , let $\Lambda(t) = \left\{ (x(\alpha, t), \xi(\alpha, t)) \mid \alpha \in (\beta, \gamma) \right\}$, then

$$\int_{\mathbb{R}^2} f(x, \xi, 0) I_{\Lambda(0)} dx d\xi = \int_{\mathbb{R}^2} f(x, \xi, t) I_{\Lambda(t)} dx d\xi = \int_{\beta}^{\gamma} \varrho_0(\alpha) d\alpha, \quad \forall t. \quad (2.13)$$

Proof. For all $\psi \in C_0^\infty(\mathbb{R} \times \mathbb{R} \times [0, T])$, since

$$\frac{dx(\alpha, t)}{dt} = \xi(\alpha, t), \quad \frac{d\xi(\alpha, t)}{dt} = -\nabla_x V,$$

it follows that

$$\begin{aligned} \frac{d\psi(x(\alpha, t), \xi(\alpha, t), t)}{dt} &= \frac{\partial\psi(x(\alpha, t), \xi(\alpha, t), t)}{\partial t} + \xi(\alpha, t) \cdot \nabla_x \psi(x(\alpha, t), \xi(\alpha, t), t) \\ &\quad - \nabla_x V \cdot \nabla_\xi \psi(x(\alpha, t), \xi(\alpha, t), t). \end{aligned}$$

Therefore

$$\begin{aligned} &\int_0^T \int_{\mathbb{R}^2} (\psi f_t + \psi \xi \cdot \nabla_x f - \psi \nabla_x V \cdot \nabla_\xi f) dx d\xi dt \\ &= - \int_0^T \int_{\mathbb{R}^2} (\psi_t f + f \xi \cdot \nabla_x \psi - f \nabla_x V \cdot \nabla_\xi \psi) dx d\xi dt \\ &= - \int_0^T \int_{\mathbb{R}} \left[\frac{\partial\psi(x(\alpha, t), \xi(\alpha, t), t)}{\partial t} + \xi(\alpha, t) \cdot \nabla_x \psi(x(\alpha, t), \xi(\alpha, t), t) \right. \\ &\quad \left. - \nabla_x V \cdot \nabla_\xi \psi(x(\alpha, t), \xi(\alpha, t), t) \right] \varrho_0(\alpha) \left| \frac{dC(\alpha, t)}{d\alpha} \right|^{-1} \left| \frac{dC(\alpha, t)}{d\alpha} \right| d\alpha dt \\ &= - \int_0^T \int_{\mathbb{R}} \frac{d\psi(x(\alpha, t), \xi(\alpha, t), t)}{dt} \varrho_0(\alpha) d\alpha dt = 0. \end{aligned}$$

□

We now explain the relationship between $f(t, x, \xi)$ and the physical observables. First, for the mono-kinetic initial data

$$f(0, x, \xi) = \rho_0(x) \delta(\xi - \nabla_x S_0(x)) = \rho_0(x) \left| \frac{dC(x)}{dx} \right|^{-1} \vartheta_C,$$

$\rho_0(x)$ is the local density, that is,

$$\rho_0(x) = \int_{-\infty}^{\infty} f(0, x, \xi) d\xi. \quad (2.14)$$

If we fix x , then $f(0, x, \xi)$ is a Dirac-delta function with respect to ξ supported on the point $\nabla_x S_0(x)$.

Next, we consider the general case, where $f(t, x, \xi)$ is a measure supported on $C(\alpha, t)$, and $C(\alpha, t)$ is not necessarily a graph in the x - ξ plane. We claim the following theorem

Theorem 2.2. *Consider a solution of (1.1) with the following form*

$$f(t, x, \xi) = \varrho_0(\alpha) \left| \frac{dC(\alpha, t)}{d\alpha} \right|^{-1} \vartheta_{C(\alpha, t)}. \quad (2.15)$$

$\forall w \in \mathbb{R}$, such that $x(\alpha, t) = w$ has finite many solutions which are denoted by

$$\alpha_1(w), \alpha_2(w), \dots, \alpha_k(w),$$

that is

$$x(\alpha_1(w), t) = x(\alpha_2(w), t) = \dots = x(\alpha_k(w), t) = w, \quad (2.16)$$

and

$$\left. \frac{\partial x}{\partial \alpha} \right|_{\alpha=\alpha_j(w)} \neq 0, \quad j = 1, \dots, k, \quad (2.17)$$

there exists $\kappa > 0$, such that

$$f(t, z, \xi) = \sum_{j=1}^k \varrho_0(\alpha_j(z)) \left| \frac{\partial x}{\partial \alpha} \right|_{\alpha=\alpha_j(z)}^{-1} \delta(\xi - \xi(\alpha_j(z))), \quad \forall z \in (w - \kappa, w + \kappa). \quad (2.18)$$

Proof. For every fixed w satisfies (2.16) and (2.17), there exists $\tau > 0$, such that $x(\alpha, t)$ is one-to-one on $(\alpha_j(w) - \tau, \alpha_j(w) + \tau)$, $j = 1, \dots, k$. Denote

$$g_j(\alpha) = x(\alpha, t), \quad \alpha \in (\alpha_j(w) - \tau, \alpha_j(w) + \tau), \quad j = 1, \dots, k. \quad (2.19)$$

Consequently, there exists $\kappa > 0$, such that $\forall z \in (w - \kappa, w + \kappa)$, the equation $x(\alpha, t) = z$ yields exactly k solutions $\alpha_1(z), \dots, \alpha_k(z)$, such that

$$\alpha_j(z) \in (\alpha_j(w) - \tau, \alpha_j(w) + \tau), \quad j = 1, \dots, k. \quad (2.20)$$

See the graph below. Therefore, $\forall z \in (w - \kappa, w + \kappa)$ and $\forall \psi \in C_0^\infty(\mathbb{R}^2)$, we have

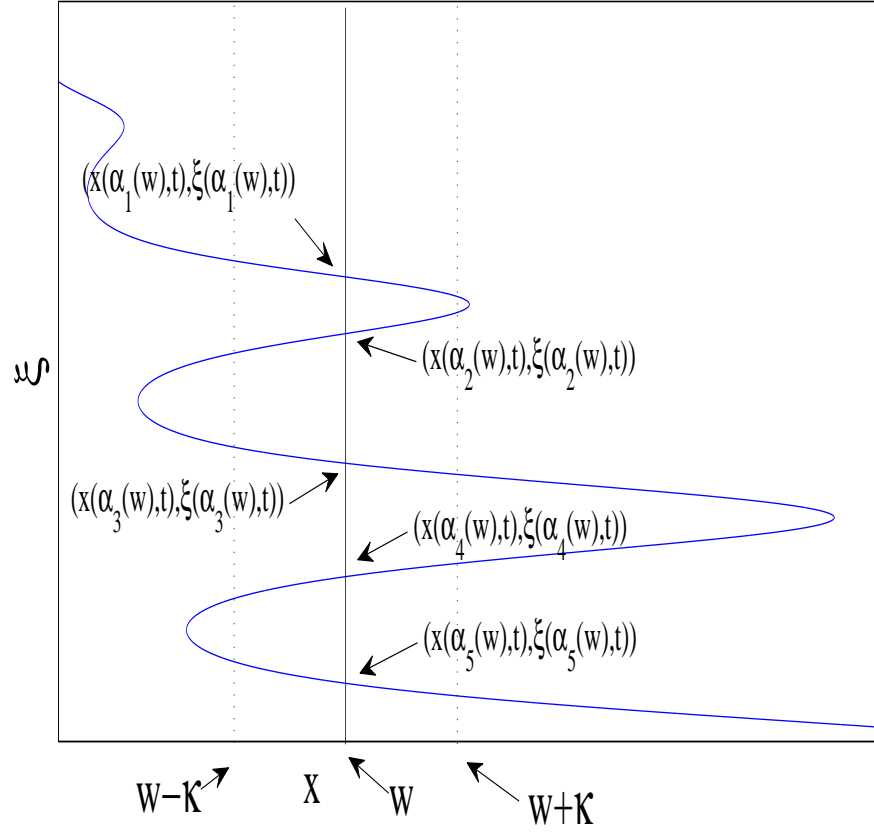


Figure 1: A simple illustration of (2.20)

$$\begin{aligned}
 & \int_{-\infty}^{\infty} \psi(z, \xi) f(t, z, \xi) d\xi \\
 = & \frac{\partial}{\partial z} \int_{-\infty}^z \int_{-\infty}^{\infty} \psi(x, \xi) f(t, x, \xi) d\xi dx \\
 = & \frac{\partial}{\partial z} \int_{w-\kappa}^z \int_{-\infty}^{\infty} \psi(x, \xi) f(t, x, \xi) d\xi dx \\
 = & \frac{\partial}{\partial z} \int_{w-\kappa}^z \int_{-\infty}^{\infty} \psi(x, \xi) \varrho(\alpha) \left| \frac{dC(\alpha)}{d\alpha} \right|^{-1} \vartheta_C d\xi dx \\
 = & \frac{\partial}{\partial z} \left(\sum_{j=1}^k \text{sign}(g_j^{-1}(z) - g_j^{-1}(w - \kappa)) \int_{g_j^{-1}(w-\kappa)}^{\alpha_j(z)=g_j^{-1}(z)} \psi(x(\alpha), \xi(\alpha)) \varrho(\alpha) \left| \frac{dC(\alpha)}{d\alpha} \right|^{-1} \left| \frac{dC(\alpha)}{d\alpha} \right| d\alpha \right) \\
 = & \frac{\partial}{\partial z} \left(\sum_{j=1}^k \text{sign}(g_j^{-1}(z) - g_j^{-1}(w - \kappa)) \int_{g_j^{-1}(w-\kappa)}^{\alpha_j(z)=g_j^{-1}(z)} \psi(x(\alpha), \xi(\alpha)) \varrho(\alpha) d\alpha \right) \\
 = & \sum_{j=1}^k \text{sign}(g_j^{-1}(z) - g_j^{-1}(w - \kappa)) \frac{\partial(g_j^{-1}(z))}{\partial z} \psi(x(\alpha_j(z)), \xi(\alpha_j(z))) \varrho(\alpha_j(z)) \\
 = & \sum_{j=1}^k \left| \frac{\partial x}{\partial \alpha} \right|_{\alpha=\alpha_j(z)}^{-1} \psi(x(\alpha_j(z)), \xi(\alpha_j(z))) \varrho_0(\alpha_j(z)). \\
 = & \sum_{j=1}^k \psi(z, \xi(\alpha_j(z))) \left| \frac{\partial x}{\partial \alpha} \right|_{\alpha=\alpha_j(z)}^{-1} \varrho_0(\alpha_j(z))
 \end{aligned}$$

□

Remark 2.4. If there are infinite but countably many solutions of $x(\alpha) = z$, then there exists $\frac{\partial x}{\partial \alpha}|_{\alpha=\alpha_j(z)} = 0$, and the local density $\rho(z, t) = \infty$. If the set $\{\alpha|x(\alpha, t) = z\}$ is not discrete, i.e., its measure in \mathbb{R} is greater than 0, then the local density $\rho(z, t)$ is a Dirac mass.

We define

$$\tilde{\rho}(\alpha, t) := \left| \frac{\partial x(\alpha, t)}{\partial \alpha} \right|^{-1} \varrho_0(\alpha). \quad (2.21)$$

Then

$$f(t, z, \xi) = \sum_{j=1}^k \tilde{\rho}(\alpha_j(z), t) \delta(\xi - \xi(\alpha_j(z), t)). \quad (2.22)$$

Thus the physical observables at $x = z$ are

$$\rho(z, t) = \int_{-\infty}^{\infty} f(t, z, \xi) d\xi = \sum_{j=1}^k \tilde{\rho}(\alpha_j(z), t), \quad (2.23)$$

$$\rho u^m(z, t) = \int_{-\infty}^{\infty} \xi^m f(t, z, \xi) d\xi = \sum_{j=1}^k \tilde{\rho}(\alpha_j(z), t) \xi(\alpha_j(z), t)^m. \quad (2.24)$$

Suppose $x(\alpha, t)$ is one-to-one on (β, γ) . Denote its inverse on (β, γ) by $\alpha(z) = x^{-1}(z)$. Let

$$\Lambda = \left\{ (x(\alpha, t), \xi(\alpha, t)) \mid \alpha \in (\beta, \gamma) \right\}, \quad (2.25)$$

then

$$\begin{aligned} & \int_{-\infty}^{\infty} \int_{-\infty}^{\infty} I_{\Lambda} f(t, z, \xi) d\xi dx \\ &= \int_{\beta}^{\gamma} \varrho_0(\alpha) \left| \frac{dC(\alpha, t)}{d\alpha} \right|^{-1} \left| \frac{dC(\alpha, t)}{d\alpha} \right| d\alpha \\ &= \int_{\beta}^{\gamma} \varrho_0(\alpha) d\alpha \\ &= \int_{x(\beta)}^{x(\gamma)} \varrho_0(x^{-1}(z)) \left(\frac{\partial x^{-1}}{\partial z} \right) dz \quad \alpha(z) = x^{-1}(z) \\ &= \text{sign}(x(\gamma) - x(\beta)) \int_{x(\beta)}^{x(\gamma)} \tilde{\rho}(\alpha(z), t) dz. \end{aligned} \quad (2.26)$$

Let

$$M(\varpi) = \int_0^{\varpi} \varrho_0(\alpha) d\alpha, \quad (2.27)$$

then

$$\text{sign}(x(\gamma) - x(\beta)) \int_{x(\beta, t)}^{x(\gamma, t)} \tilde{\rho}(\alpha(z), t) dz = M(\gamma) - M(\beta) = \int_{\beta}^{\gamma} \varrho_0(\alpha) d\alpha. \quad (2.28)$$

We summarize the result here. To calculate the physical observables, one needs the following information: (i) the curve $C(\alpha, t)$ and (ii) $\tilde{\rho}(\alpha, t)$. Then to find the moment $\rho u^m(z, t)$ at z , we solve $x(\alpha, t) = z$, suppose there are k solutions $\alpha_1, \dots, \alpha_k$, then

$$\rho u^m(z, t) = \sum_{j=1}^k \tilde{\rho}(\alpha_j, t) \xi^m(\alpha_j, t). \quad (2.29)$$

The detailed numerical algorithm is given in Section 3.

2.2. Multi-dimensional case.

Now, we extend Definition 2.1 to surface measure supported on a hyperplane in multi-dimensional space.

Definition 2.2. Let P be a hyperplane in the $\mathbf{x}-\boldsymbol{\xi}$ space, $\mathbf{x} \in \mathbb{R}^d, \boldsymbol{\xi} \in \mathbb{R}^d$. Let $P(\boldsymbol{\alpha}) = \left\{ (\mathbf{x}(\boldsymbol{\alpha}), \boldsymbol{\xi}(\boldsymbol{\alpha})) \mid \boldsymbol{\alpha} \in \Omega \right\}$ be a parameterized form of P . The function $\eta_P(\mathbf{x}, \boldsymbol{\xi})$ is a surface measure supported on the hyperplane P , defined by

$$\int_{\mathbb{R}^{2d}} \psi(\mathbf{x}, \boldsymbol{\xi}) \eta_P(\mathbf{x}, \boldsymbol{\xi}) d\boldsymbol{\xi} d\mathbf{x} = \int_{\Omega} \psi(\mathbf{x}(\boldsymbol{\alpha}), \boldsymbol{\xi}(\boldsymbol{\alpha})) \frac{dA(\boldsymbol{\alpha})}{d\boldsymbol{\alpha}} d\boldsymbol{\alpha}, \quad \forall \psi \in C_0^\infty(\mathbb{R}^{2d}), \quad (2.30)$$

where $\int_{\Lambda} \frac{dA(\boldsymbol{\alpha})}{d\boldsymbol{\alpha}} d\boldsymbol{\alpha}$ is the area of the hyperplane $P(\boldsymbol{\alpha} \in \Lambda)$, $\forall \Lambda \subset \Omega$.

Remark 2.5. It is easy to verify that definition 2.2 is independent of the choice of the parametrization $\boldsymbol{\alpha}$.

In general, the hyperplane has dimension $0 \leq k \leq 2d$, with $\Omega \subset \mathbb{R}^k$. The mono-kinetic initial data (1.7) is a special case of (2.30), where the hyperplane has dimension d . More precisely, (1.7) is equivalent to a measure supported on a hyperplane $P(\mathbf{x}, \nabla_{\mathbf{x}} S_0(\mathbf{x}))$ such that the local density $\int_{\mathbb{R}^d} f d\boldsymbol{\xi} = \rho_0(\mathbf{x})$, that is,

$$f(0, \mathbf{x}, \boldsymbol{\xi}) = \rho_0(\mathbf{x}) \left(\frac{dA}{d\mathbf{x}} \right)^{-1} \eta_P(\mathbf{x}, \boldsymbol{\xi}).$$

We verify it below: $\forall \psi \in C_0^\infty(\mathbb{R}^{2d})$,

$$\begin{aligned} \int_{\mathbb{R}^{2d}} \psi(\mathbf{x}, \boldsymbol{\xi}) \rho_0(\mathbf{x}) \delta(\boldsymbol{\xi} - \nabla_{\mathbf{x}} S_0(\mathbf{x})) d\boldsymbol{\xi} d\mathbf{x} &= \int_{\mathbb{R}^d} \psi(\mathbf{x}, \nabla_{\mathbf{x}} S_0(\mathbf{x})) \rho_0(\mathbf{x}) d\mathbf{x}, \\ \int_{\mathbb{R}^{2d}} \psi(\mathbf{x}, \boldsymbol{\xi}) \rho_0(\mathbf{x}) \left(\frac{dA}{d\mathbf{x}} \right)^{-1} \eta_P(\mathbf{x}, \boldsymbol{\xi}) d\boldsymbol{\xi} d\mathbf{x} &= \int_{\mathbb{R}^d} \psi(\mathbf{x}, \nabla_{\mathbf{x}} S_0(\mathbf{x})) \rho_0(\mathbf{x}) \left(\frac{dA}{d\mathbf{x}} \right)^{-1} \left(\frac{dA}{d\mathbf{x}} \right) d\mathbf{x}. \end{aligned}$$

Thus

$$\int_{\mathbb{R}^{2d}} \psi(\mathbf{x}, \boldsymbol{\xi}) \rho_0(\mathbf{x}) \delta(\boldsymbol{\xi} - \nabla_{\mathbf{x}} S_0(\mathbf{x})) d\boldsymbol{\xi} d\mathbf{x} = \int_{\mathbb{R}^{2d}} \psi(\mathbf{x}, \boldsymbol{\xi}) \rho_0(\mathbf{x}) \left(\frac{dA}{d\mathbf{x}} \right)^{-1} \eta_P(\mathbf{x}, \boldsymbol{\xi}) d\boldsymbol{\xi} d\mathbf{x}.$$

In general, we do not require P to be a graph in $\mathbf{x}-\boldsymbol{\xi}$ space with dimension d . Let $g(\mathbf{x}, \boldsymbol{\xi}) = p(\mathbf{x}, \boldsymbol{\xi}) \eta_P$ be a surface measure supported on P . Then the value of p on P determines the measure g . More precisely, $p(\boldsymbol{\alpha}) := p(\mathbf{x}(\boldsymbol{\alpha}), \boldsymbol{\xi}(\boldsymbol{\alpha}))$, $\boldsymbol{\alpha} \in \Omega$, determines g . Therefore, for $P(\boldsymbol{\alpha}) = \left\{ (\mathbf{x}(\boldsymbol{\alpha}), \boldsymbol{\xi}(\boldsymbol{\alpha})) \mid \boldsymbol{\alpha} \in \Omega \right\}$, we simply denote g as

$$g(\boldsymbol{\alpha}) = p(\boldsymbol{\alpha}) \eta_{P(\boldsymbol{\alpha})}.$$

Theorem 2.3. Consider (1.1) with measure initial data, i.e., a measure supported on a hyperplane with dimension k which has the form $P(\boldsymbol{\alpha}, 0) = (\mathbf{x}_0(\boldsymbol{\alpha}), \boldsymbol{\xi}_0(\boldsymbol{\alpha}))$, $\boldsymbol{\alpha} \in \Omega \subset \mathbb{R}^k$, with weight $p(\boldsymbol{\alpha}, 0) = \varrho_0(\boldsymbol{\alpha}) \left| \frac{dA(\boldsymbol{\alpha}, 0)}{d\boldsymbol{\alpha}} \right|^{-1}$. Denote the solution of the initial value problem to the Hamiltonian system

$$\frac{d\mathbf{x}}{dt} = \boldsymbol{\xi}, \quad \frac{d\boldsymbol{\xi}}{dt} = -\nabla_{\mathbf{x}}V, \quad \mathbf{x}(0) = \mathbf{x}_0(\boldsymbol{\alpha}), \quad \boldsymbol{\xi}(0) = \boldsymbol{\xi}_0(\boldsymbol{\alpha}), \quad (2.31)$$

by $(\mathbf{x}(\boldsymbol{\alpha}, t), \boldsymbol{\xi}(\boldsymbol{\alpha}, t))$. Then a measure supported on the hyperplane $P(\boldsymbol{\alpha}, t) = (\mathbf{x}(\boldsymbol{\alpha}, t), \boldsymbol{\xi}(\boldsymbol{\alpha}, t))$, $\boldsymbol{\alpha} \in \Omega$, with the weight given by

$$p(\boldsymbol{\alpha}, t) = \varrho_0(\boldsymbol{\alpha}) \left| \frac{dA(\boldsymbol{\alpha}, t)}{d\boldsymbol{\alpha}} \right|^{-1},$$

is a weak solution to (1.1) with the given initial data. Let $P_\Lambda(t) = \{(\mathbf{x}(\boldsymbol{\alpha}, t), \boldsymbol{\xi}(\boldsymbol{\alpha}, t)) \mid \boldsymbol{\alpha} \in \Lambda \subset \mathbb{R}^k\}$. Then

$$\int_{\mathbb{R}^{2d}} f(\mathbf{x}, \boldsymbol{\xi}, 0) I_{P_\Lambda(0)} d\mathbf{x} d\boldsymbol{\xi} = \int_{\mathbb{R}^{2d}} f(\mathbf{x}, \boldsymbol{\xi}, t) I_{P_\Lambda(t)} d\mathbf{x} d\boldsymbol{\xi}, \quad \forall \Lambda \subset \Omega, \quad \forall t, \quad (2.32)$$

that is,

$$\int_\Lambda p(\boldsymbol{\alpha}, 0) \frac{dA(\boldsymbol{\alpha}, 0)}{d\boldsymbol{\alpha}} d\boldsymbol{\alpha} = \int_\Lambda p(\boldsymbol{\alpha}, t) \frac{dA(\boldsymbol{\alpha}, t)}{d\boldsymbol{\alpha}} d\boldsymbol{\alpha}. \quad (2.33)$$

Proof. $\forall \psi \in C_0^\infty(\mathbb{R}^d \times \mathbb{R}^d \times [0, T])$,

$$\begin{aligned} & \int_0^T \int_{\mathbb{R}^{2d}} (\psi f_t + \psi \boldsymbol{\xi} \cdot \nabla_{\mathbf{x}} f - \psi \nabla_{\mathbf{x}} V \cdot \nabla_{\boldsymbol{\xi}} f) d\mathbf{x} d\boldsymbol{\xi} dt \\ &= - \int_0^T \int_{\mathbb{R}^{2d}} (\psi_t f + f \boldsymbol{\xi} \cdot \nabla_{\mathbf{x}} \psi - f \nabla_{\mathbf{x}} V \cdot \nabla_{\boldsymbol{\xi}} \psi) d\mathbf{x} d\boldsymbol{\xi} dt \\ &= - \int_0^T \int_{\mathbb{R}^k} \left[\frac{\partial \psi(\mathbf{x}(\boldsymbol{\alpha}, t), \boldsymbol{\xi}(\boldsymbol{\alpha}, t), t)}{\partial t} + \boldsymbol{\xi}(\boldsymbol{\alpha}, t) \cdot \nabla_{\mathbf{x}} \psi(\mathbf{x}(\boldsymbol{\alpha}, t), \boldsymbol{\xi}(\boldsymbol{\alpha}, t), t) \right. \\ & \quad \left. - \nabla_{\mathbf{x}} V \cdot \nabla_{\boldsymbol{\xi}} \psi(\mathbf{x}(\boldsymbol{\alpha}, t), \boldsymbol{\xi}(\boldsymbol{\alpha}, t), t) \right] \varrho_0(\boldsymbol{\alpha}) \left| \frac{dA(\boldsymbol{\alpha}, t)}{d\boldsymbol{\alpha}} \right|^{-1} \left| \frac{dA(\boldsymbol{\alpha}, t)}{d\boldsymbol{\alpha}} \right| d\boldsymbol{\alpha} dt \\ &= - \int_0^T \int_{\mathbb{R}^k} \frac{d\psi(\mathbf{x}(\boldsymbol{\alpha}, t), \boldsymbol{\xi}(\boldsymbol{\alpha}, t), t)}{dt} \varrho_0(\boldsymbol{\alpha}) d\boldsymbol{\alpha} dt = 0. \end{aligned}$$

Here we used the fact that

$$\frac{d\mathbf{x}(\boldsymbol{\alpha}, t)}{dt} = \boldsymbol{\xi}(\boldsymbol{\alpha}, t), \quad \frac{d\boldsymbol{\xi}(\boldsymbol{\alpha}, t)}{dt} = -\nabla_{\mathbf{x}}V,$$

therefore

$$\begin{aligned} \frac{d\psi(\mathbf{x}(\boldsymbol{\alpha}, t), \boldsymbol{\xi}(\boldsymbol{\alpha}, t), t)}{dt} &= \frac{\partial \psi(\mathbf{x}(\boldsymbol{\alpha}, t), \boldsymbol{\xi}(\boldsymbol{\alpha}, t), t)}{\partial t} + \boldsymbol{\xi}(\boldsymbol{\alpha}, t) \cdot \nabla_{\mathbf{x}} \psi(\mathbf{x}(\boldsymbol{\alpha}, t), \boldsymbol{\xi}(\boldsymbol{\alpha}, t), t) \\ & \quad - \nabla_{\mathbf{x}} V \cdot \nabla_{\boldsymbol{\xi}} \psi(\mathbf{x}(\boldsymbol{\alpha}, t), \boldsymbol{\xi}(\boldsymbol{\alpha}, t), t). \end{aligned}$$

□

Consider the Liouville equation with initial data (1.7), that is $\Omega \subset \mathbb{R}^d$. Similar to the one-dimensional case, denote $\tilde{\rho}(\boldsymbol{\alpha}, t) := \left| \frac{\partial \mathbf{x}(\boldsymbol{\alpha}, t)}{\partial \boldsymbol{\alpha}} \right|^{-1} \varrho_0(\boldsymbol{\alpha})$, then $f(t, \mathbf{x}, \boldsymbol{\xi})$ can be rewritten as

$$f(t, \mathbf{z}, \boldsymbol{\xi}) = \sum_{j=1}^k \tilde{\rho}(\boldsymbol{\alpha}_j(\mathbf{z}), t) \delta(\boldsymbol{\xi} - \boldsymbol{\xi}(\boldsymbol{\alpha}_j(\mathbf{z}), t)), \quad (2.34)$$

where $\boldsymbol{\alpha}_1(\mathbf{z}), \dots, \boldsymbol{\alpha}_k(\mathbf{z})$ are solutions of $\mathbf{x}(\boldsymbol{\alpha}, t) = \mathbf{z}$. Moreover, if $\mathbf{x}(\boldsymbol{\alpha}, t)$ is one-to-one on $\boldsymbol{\alpha} \in \Omega_1 \subset \Omega$, then

$$\int_{\mathbf{x}(\Omega_1)} \tilde{\rho}(\mathbf{x}^{-1}(\mathbf{z}), t) d\mathbf{z} = \int_{\Omega_1} \varrho_0(\boldsymbol{\alpha}) d\boldsymbol{\alpha}. \quad (2.35)$$

3. THE DETAILED NUMERICAL IMPLEMENTATION

3.1. The one-dimensional numerical implementation.

We now describe the numerical details for the one-dimensional Liouville equation. Suppose the initial data is given by

$$f(0, x, \xi) = \varrho_0(\alpha) \left| \frac{dC(\alpha, 0)}{d\alpha} \right|^{-1} \vartheta_{C(\alpha, 0)}. \quad (3.1)$$

Without loss of generality, we assume $\alpha \in (0, 1)$.

Step 1. Let $\alpha_j = \frac{j}{N}$, $j = 0, \dots, N$.

Step 2. Evaluate the initial charge

$$m_j = \int_{\alpha_{j-1}}^{\alpha_j} \varrho_0(\alpha) d\alpha \quad j = 1, \dots, N,$$

numerically by some quadrature rule or analytically if possible.

Step 3. Solve

$$\frac{dx_j(t)}{dt} = \xi_j, \quad \frac{d\xi_j(t)}{dt} = -V_x, \quad x_j(0) = x(\alpha_j, 0), \quad \xi_j(0) = \xi(\alpha_j, 0),$$

numerically to obtain $x_j(T), u_j(T)$, $j = 0, \dots, N$.

Step 4. Approximate $C(\alpha, T)$. For example, if a piecewise linear approximation is used, one gets

$$x(\alpha, T) = x_{j-1}(T) + \frac{\alpha - \alpha_{j-1}}{N} (x_j(T) - x_{j-1}(T)), \quad (3.2a)$$

$$\xi(\alpha, t) = \xi_{j-1}(T) + \frac{\alpha - \alpha_{j-1}}{N} (\xi_j(T) - \xi_{j-1}(T)), \quad (3.2b)$$

$$\alpha \in (\alpha_{j-1}, \alpha_j), \quad j = 1, \dots, N.$$

This also gives a multi-valued solution of the velocity \tilde{u} , that is,

$$\tilde{u}(x(\alpha, t), t) = \xi(\alpha, t), \quad \alpha \in (0, 1). \quad (3.3)$$

\tilde{u} can be multi-valued since it is possible that $x(\beta_1, t) = x(\beta_2, t)$ for $\beta_1 \neq \beta_2$.

Step 5. By (2.28)

$$\text{sign}(x(\alpha_{j+1}, T) - x(\alpha_j, T)) \int_{x(\alpha_j, T)}^{x(\alpha_{j+1}, T)} \tilde{\rho}(\alpha(z), t) dz = M(\alpha_{j+1}) - M(\alpha_j) = m_j. \quad (3.4)$$

We use a constant to approximate $\tilde{\rho}(\alpha, T)$ on $\alpha \in (\alpha_j, \alpha_{j+1})$. That is,

$$\tilde{\rho}(\alpha, T) \approx \frac{m_j}{|x(\alpha_{j+1}, T) - x(\alpha_j, T)|}, \quad \alpha \in (\alpha_j, \alpha_{j+1}). \quad (3.5)$$

Similar to \tilde{u} , $\tilde{\rho}$ gives a multi-valued solution of density. The (single valued) position density is given by

$$\rho(y, T) = \sum_{j=0}^{N-1} \frac{m_j}{|x(\alpha_{j+1}, T) - x(\alpha_j, T)|} I_{(x(\alpha_j, T), x(\alpha_{j+1}, T))}(y). \quad (3.6)$$

Step 6. Compute any desired physical observables by using the results of Step 4 and 5. For example

$$\rho(y, T)u(y, T) = \sum_{p=1}^k \tilde{\rho}(\alpha_p(y), T)\xi(\alpha_p(y), T), \quad (3.7)$$

where $\alpha_p(y)$ are solutions of $x(\alpha, T) = y$. By (3.2), if $y \in (x(\alpha_j, T), x(\alpha_{j+1}, T))$, then $\alpha = \frac{y-x_j(T)}{x_{j+1}(T)-x_j(T)}N + \alpha_j$ is a solution of $x(\alpha, T) = y$, and $\xi(\alpha, t) = \xi_j(T) + \frac{(y-x_j(T))(\xi_{j+1}(T)-\xi_j(T))}{x_{j+1}(T)-x_j(T)}$. Therefore

$$\begin{aligned} \rho(y, T)u(y, T) = \\ \sum_{j=0}^{N-1} \frac{m_j}{|x(\alpha_{j+1}, T) - x(\alpha_j, T)|} I_{(x(\alpha_j, T), x(\alpha_{j+1}, T))}(y) \left(\xi_j(T) + \frac{(y - x_j(T))(\xi_{j+1}(T) - \xi_j(T))}{x_{j+1}(T) - x_j(T)} \right). \end{aligned} \quad (3.8)$$

3.2. The multi-dimensional numerical implementation.

We briefly describe the multi-dimensional procedure with the use of (2.33)

Step 1. Decompose Ω into N subdomains, $\Omega_1, \Omega_2, \dots, \Omega_N$, each has $k + 1$ vertices, which are initial particle positions.

Step 2. Evaluate the initial charge

$$m_j = \int_{\Omega_j} p(\boldsymbol{\alpha}, 0) \frac{dA(\boldsymbol{\alpha}, 0)}{d\boldsymbol{\alpha}} d\boldsymbol{\alpha} \quad j = 1, \dots, N,$$

numerically by some quadrature rule or analytically if possible.

Step 3. Follow all particles by numerically solving

$$\frac{d\mathbf{x}(t)}{dt} = \boldsymbol{\xi}, \quad \frac{d\boldsymbol{\xi}(t)}{dt} = -\nabla_{\mathbf{x}}V, \quad \mathbf{x}(0) = \mathbf{x}(\boldsymbol{\alpha}, 0), \quad \boldsymbol{\xi}(0) = \boldsymbol{\xi}(\boldsymbol{\alpha}, 0), \quad (3.9)$$

Step 4. Approximate $P(\boldsymbol{\alpha}, T)$ by a piecewise linear function. That is, connecting vertices at time T in the original order to approximate $\Omega_j(T)$. Use the linear interpolation to approximate $\boldsymbol{\xi}(\boldsymbol{\alpha}, T)$ for $\boldsymbol{\alpha} \in \Omega_j(0)$.

Step 5. Approximate $\tilde{\rho}(\boldsymbol{\alpha}, T)$ on $\boldsymbol{\alpha} \in \Omega_j(0)$ by a constant, that is, let

$$\tilde{\rho}(\boldsymbol{\alpha}, T) = \frac{m_j}{|\Omega_j(T)|}, \quad \boldsymbol{\alpha} \in \Omega_j(0).$$

Step 6. Calculate any desired physical observables by taking the moments of $f(\mathbf{x}, \boldsymbol{\xi}, T)$. For a 2D example of this step, see section 3.3.

Remark 3.1. When using the deterministic particle methods, point values of the computed solutions have to be recovered from their singular particle approximations by using some smoothing procedure (for details, see section 5.1). Our method avoids this recovery step, thus it is simpler and more accurate. Moreover, our solution will remain a surface measure supported on a hyperplane with dimension k provided the initial data is such. Therefore, no matter how singular the initial data is, we keep the detailed structure of the singular solution. The reason is that our mesh points is on Ω , not the $\mathbf{x} - \boldsymbol{\xi}$ space.

3.3. A detailed implementation of the 2D Algorithm.

In this subsection, we give a detailed numerical implementation for the 2D Liouville equation with initial data (1.7). Numerical methods for the higher dimensional Liouville equation can be constructed similarly.

Without loss of generality, assume $\mathbf{x} = (x, y) \in [0, 1] \times [0, 1]$, $\boldsymbol{\xi} \in \mathbb{R}^2$.

Step 1. Given mesh size $\Delta x = \Delta y = 1/N$. Denote $\mathbf{x}(j, l) = (x_j, y_l)$.

Step 2. There are N^2 cells. Denote the cell $(x_j, x_{j+1}) \times (y_l, y_{l+1})$ by $\Omega_k(0)$, where $k = (j+1 + lN)$. Since the elementary elements in 2D are triangles, we further split $\Omega_k(0)$ into two parts $\Omega_{k1}(0)$ and $\Omega_{k2}(0)$, where $\Omega_{k1}(0)$ is the triangle with vertices $\mathbf{x}(j, l)$, $\mathbf{x}(j+1, l)$, $\mathbf{x}(j, l+1)$, and $\Omega_{k2}(0)$ is the triangle with vertices $\mathbf{x}(j, l+1)$, $\mathbf{x}(j+1, l)$, $\mathbf{x}(j+1, l+1)$. Evaluate the initial charge

$$m_{kq} = \int \int_{\Omega_{kq}} \rho_0(x, y) dx dy \quad k = 1, \dots, N^2, \quad q = 1, 2,$$

numerically by some quadrature rule or analytically if possible.

Step 3. Solve numerically

$$\frac{d\mathbf{x}_{jl}(t)}{dt} = \boldsymbol{\xi}_{jl}, \quad \frac{d\boldsymbol{\xi}_{jl}(t)}{dt} = -\nabla_{\mathbf{x}} V,$$

subject to the initial data

$$\mathbf{x}_{jl}(0) = (x_j, y_l) \quad \boldsymbol{\xi}_{jl}(0) = \nabla_{\mathbf{x}} S_0(\mathbf{x}_{jl}(0)),$$

to obtain $\mathbf{x}_{jl}(T)$, $\boldsymbol{\xi}_{jl}(T)$, $j = 0, \dots, N$, $l = 0, \dots, N$.

Step 4. Apply the linear interpolation to approximate velocity on $\Omega_{kq}(T)$. More precisely, denote the vertices of Ω_{kq} by \mathbf{a} , \mathbf{b} , \mathbf{c} , and the velocity at them are \mathbf{u}_a , \mathbf{u}_b , \mathbf{u}_c respectively. Then for every $\mathbf{x} \in \Omega_{kq}$, one can decompose $\mathbf{x} - \mathbf{a}$ uniquely as

$$\mathbf{x} - \mathbf{a} = \mu(\mathbf{b} - \mathbf{a}) + \nu(\mathbf{c} - \mathbf{a}),$$

here (μ, ν) can be solved analytically, and interpolate

$$\boldsymbol{\xi}(\mathbf{x}, t) = \mathbf{u}_a + \mu(\mathbf{u}_b - \mathbf{u}_a) + \nu(\mathbf{u}_c - \mathbf{u}_a).$$

This gives a multi-valued solution of velocity $\tilde{\mathbf{u}}$ at time T . Denote $\boldsymbol{\xi}(\mathbf{x}, t)$ on Ω_{kq} by $\boldsymbol{\xi}_{kq}(\mathbf{x}, t)$.

Step 5. Denote the area of the triangle $\Omega_{kq}(T)$ by $A_{kq}(T)$. Let $\tilde{\rho}(\boldsymbol{\alpha}, T) = \frac{m_{kq}}{A_{kq}(T)}$ on (associated with) $\Omega_{kq}(T)$. This gives a multi-valued solution of density at time T . The (single valued) position density then follows

$$\rho(\mathbf{x}, T) = \sum_{q=1}^2 \sum_{k=1}^{N^2} \frac{m_{kq}}{A_{kq}(T)} I_{\Omega_{kq}(T)}(\mathbf{x}) \quad (3.10)$$

Step 6. Compute any desired physical variables by using the result of Steps 4 and 5. For example

$$\rho(\mathbf{x}, T)u(\mathbf{x}, T) = \sum_{q=1}^2 \sum_{k=1}^{N^2} \frac{m_{kq}}{A_{kq}(T)} I_{\Omega_{kq}(T)}(\mathbf{x}) \boldsymbol{\xi}_{kq}(\mathbf{x}, T). \quad (3.11)$$

Remark 3.2. One can apply any higher order numerical method in Steps 3, 4 and 5. In addition to its high efficiency and accuracy, a major advantage of the method is that it gives very accurate numerical solutions around caustics. The reason is: the particles become automatically dense when caustic develops, and the total charge inside any cell around the caustic is calculated at $t = 0$. For classical particle methods, one has to apply some smoothing procedure to recover point values of the computed solutions from their singular particle approximations, therefore, even the particles are dense around the caustics, the smoothing procedure smears the solution. For details of the smoothing procedures, see Section 5.1. In addition we give the multi-valued solution rather than the single valued physical observables.

Remark 3.3. For a 2D problem, when using (3.10) to calculate the local density ρ on a mesh $\{\mathbf{y}_{ij}\}$, one needs to identify whether \mathbf{y}_{ij} is inside a triangle or not many times. We apply the following fast test method. Denote the vertices of the triangle Ω_{kq} by $\mathbf{a}, \mathbf{b}, \mathbf{c}$, where $\mathbf{a} = (a_1, a_2)$, $\mathbf{b} = (b_1, b_2)$ and $\mathbf{c} = (c_1, c_2)$. Denote $x_{\min} = \min\{a_1, b_1, c_1\}$, $x_{\max} = \max\{a_1, b_1, c_1\}$, $y_{\min} = \min\{a_2, b_2, c_2\}$, $y_{\max} = \max\{a_2, b_2, c_2\}$. Then for every $\mathbf{y}_{ij} \in \mathbb{R}^2$, we first test whether $\mathbf{y}_{ij} \in (x_{\min}, x_{\max}) \times (y_{\min}, y_{\max})$, if not, \mathbf{y}_{ij} is outside the triangle Ω_{kq} ; otherwise we decompose $\mathbf{y}_{ij} - \mathbf{a}$ as

$$\mathbf{y}_{ij} - \mathbf{a} = \mu(\mathbf{b} - \mathbf{a}) + \nu(\mathbf{c} - \mathbf{a}),$$

then \mathbf{y}_{ij} is inside the triangle Ω_{kq} if and only if $0 < \mu < 1$, $0 < \nu < 1$ and $\mu + \nu < 1$. This procedure greatly enhances the numerical method for the Vlasov-Poisson equation to be present in the next section, since there one needs to construct ρ at every time step.

4. THE VLASOV-POISSON EQUATIONS

We can apply the new method to the Vlasov-Poisson equations

$$f_t + \mathbf{v} \cdot \nabla_{\mathbf{x}} f - \mathbf{E}(\mathbf{x}, t) \cdot \nabla_{\mathbf{v}} f = 0, \quad (4.1a)$$

$$\Delta_{\mathbf{x}} V = \int_{\mathbb{R}^d} f(\mathbf{x}, \mathbf{v}, t) d\mathbf{v} =: \rho(\mathbf{x}, t), \quad E = -\nabla_{\mathbf{x}} V, \quad (4.1b)$$

here $E(\mathbf{x}, t)$ is the electric field, V the potential.

For example, for the 1D and 2D Vlasov-Poisson equations, in each time step t to $t + \Delta t$, we do the following:

- (i) Choose a uniform mesh $\{\mathbf{y}_{ij}\}$ on \mathbf{x} -plane. The initial particles are located at the mesh points: $\mathbf{x}_{ij}(0) = \mathbf{y}_{ij}$.
- (ii) solve the characteristic equations numerically

$$\frac{d\mathbf{x}_{ij}(t)}{dt} = \boldsymbol{\xi}_{ij}, \quad \frac{d\boldsymbol{\xi}_{ij}(t)}{dt} = -E,$$

to get particle positions and velocities $\mathbf{x}_{ij}(t + \Delta t)$, $\boldsymbol{\xi}_{ij}(t + \Delta t)$;

- (iii) use (3.6) and (3.10) to calculate the local density on *uniform mesh points* $\{\mathbf{y}_{ij}\}$ at time $t + \Delta t$; then use the standard three-point center difference scheme (1D) and five-point center difference scheme (2D) to solve the Poisson equation (4.1b) to get the potential $V(t + \Delta t, \mathbf{y}_{ij})$; take finite difference of $V(t + \Delta t, \mathbf{y}_{ij})$ to get $E(t + \Delta t, \mathbf{y}_{ij})$;
- (iv) use the linear interpolation to get E on *particle positions* $\mathbf{x}_{ij}(t + \Delta t)$, which will be used in (ii) in the next time step.

Remark 4.1. Denote the particle number by M . In step (iii), the computational cost for evaluating the single valued position density ρ on uniform mesh points \mathbf{y}_{ij} of our method and all other particle methods are of the same order $O(M^2)$. In step (iv), the computational cost for evaluating E on particle positions of all methods are of order $O(M)$. Although the computational cost for all methods have the same order, our method is much faster than the previous particle methods in practice. We show a comparison in a 2D numerical example in section 5.2.

5. NUMERICAL EXAMPLES

We carry out one and two dimensional numerical experiments in this section. In these examples, we compare numerical solutions obtained by our method with solutions obtained by previous particle methods. The main difference between our proposed method and the previous particle methods is that the latter have to apply some smoothing procedures to recover point value of the numerical solution from the singular particle approximation. For reader's convenience, in Section 5.1 we briefly describe three smoothing procedures that have been studied in [4], and refer to [4] and references therein for more details.

In all examples, we solve the ODE (3.9) by the forward Euler method, although one can use any other higher order methods. The initial charge m_j was computed by the Matlab subroutines QUAD and QUAD2D, which approximate the integral by using recursive adaptive Simpson quadrature.

5.1. The smoothing procedures of particle methods.

To use the particle method, one first replaces the initial data $f(0, \mathbf{x}, \boldsymbol{\xi}) = \rho_0(\mathbf{x})\delta(\boldsymbol{\xi} - \mathbf{u}_0(\mathbf{x}))$ with a singular particle approximation. More precisely, one decomposes the computational domain Ω into M nonintersecting domains $\Omega = \Omega_1 \cup \dots \cup \Omega_M$. Then particles with masses $\int_{\Omega_i} \rho_0(\mathbf{x})d\mathbf{x}$ are placed initially at $\mathbf{x}_i(0)$, where $\mathbf{x}_i(0)$ are the coordinates of the centers of mass of Ω_i . The initial velocities of the particles are taken to be $\mathbf{u}_0(\mathbf{x}_i(0))$. That is, one replaces $f(0, \mathbf{x}, \boldsymbol{\xi}) = \rho_0(\mathbf{x})\delta(\boldsymbol{\xi} - \mathbf{u}_0(\mathbf{x}))$ with

$$\tilde{f}(0, \mathbf{x}, \boldsymbol{\xi}) = \sum_{i=1}^M \int_{\Omega_i} \rho_0(\mathbf{x})d\mathbf{x} \delta(\mathbf{x} - \mathbf{x}_i(0)) \delta(\boldsymbol{\xi} - \mathbf{u}_0(\mathbf{x}_i(0))). \quad (5.1)$$

Denote $\tilde{f}(0, \mathbf{x}, \boldsymbol{\xi})$ in its equivalent form

$$\mathbf{w}^M(\mathbf{x}, 0) = \sum_{i=1}^M \boldsymbol{\varsigma}_i(0) \delta(\mathbf{x} - \mathbf{x}_i(0)). \quad (5.2)$$

Here $\boldsymbol{\varsigma}_i(0) = (\varsigma_i^{(1)}, \dots, \varsigma_i^{(d)}, \varsigma_i^{(d+1)})(0)$, and ς_i^k is the x_k -moment ($k = 1, \dots, d$) of the i th particle, $\varsigma_i^{(d+1)}$ is the mass of the i th particle. Solving the following ODEs

$$\frac{d\mathbf{x}_i(t)}{dt} = \boldsymbol{\xi}_i(t), \quad \frac{d\boldsymbol{\xi}_i(t)}{dt} = -\nabla_{\mathbf{x}} V, \quad (5.3)$$

one obtains a singular solution at time t

$$\mathbf{w}^M(\mathbf{x}, t) = \sum_{i=1}^M \boldsymbol{\varsigma}_i(t) \delta(\mathbf{x} - \mathbf{x}_i(t)). \quad (5.4)$$

Assume one wants to find computational solutions of physical observables in $\Theta \subset \mathbb{R}^d$, the final step of the particle method is to recover the point values of the density and momenta from (5.4). Three recovery methods have been compared in [4]:

- **AVE**: The simplest way of regularizing (5.4) is to approximate it by a piecewise constant

$$\mathbf{w}(\mathbf{x}, t) = \frac{1}{|C_j|} \sum_{i=1}^M \boldsymbol{\varsigma}_i(t) \chi_{C_j}(\mathbf{x}_i(t)), \quad \mathbf{x} \in C_j.$$

Here $\{C_j\}_{j=1}^J$ is an auxiliary mesh consisting of non-overlapping cells such that $C_1 \cup \dots \cup C_J = \Theta$.

- **CONV**: This is the most widely used way of regularizing (5.4). Taking a convolution product with a smooth kernel $\zeta_\delta(x)$:

$$\mathbf{w}(\mathbf{x}, t) = (\mathbf{w}^M * \zeta_\delta)(\mathbf{x}, t) := \sum_{i=1}^M \boldsymbol{\varsigma}_i(t) \zeta_\delta(\mathbf{x} - \mathbf{x}_i(t)), \quad (5.5)$$

where ζ_δ serves as a smooth approximation of the delta-function with the following properties:

$$\zeta_\delta = \frac{1}{\delta^d} \zeta\left(\frac{\mathbf{x}}{\delta}\right), \quad \int_{\mathbb{R}^d} \zeta(\mathbf{x}) d\mathbf{x} = 1,$$

where δ is a positive parameter measuring the “width” of the kernel. In our experiments, we have used the Gaussian kernel.

- **RED**: This recovery procedure is based on the particle weights redistribution technique typically used in the immersed boundary method, [25]. In the numerical experiments of [4], the point values of \mathbf{w} have been computed at the equally spaced points where the particles were initially placed, namely:

$$\mathbf{w}(\mathbf{x}, t) = \frac{1}{\Delta x_1 \Delta x_2 \dots \Delta x_d} \sum_{i=1}^M \boldsymbol{\varsigma}_i(t) \phi\left(\frac{|x_1 - x_{i1}(t)|}{\Delta x_1}\right) \dots \phi\left(\frac{|x_d - x_{id}(t)|}{\Delta x_d}\right),$$

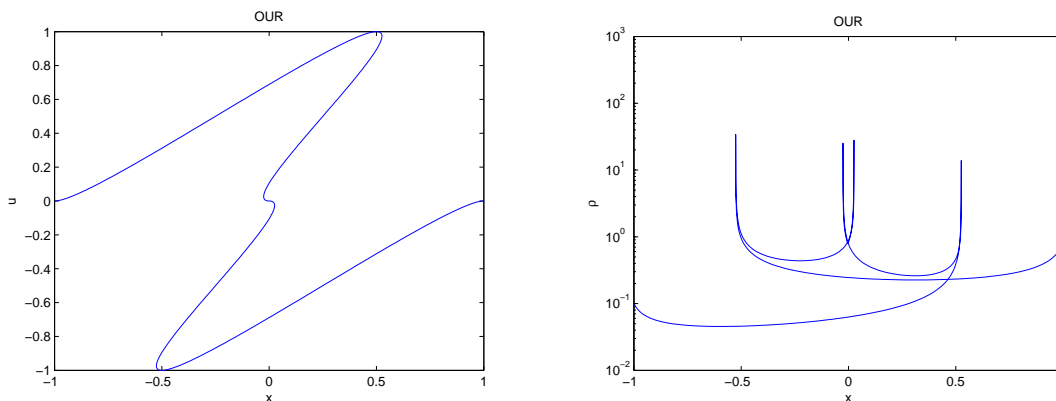


Figure 1: Example 5.1, our method with 400 particles, left: velocity \tilde{u} , right: density $\tilde{\rho}$, $t=1$.

where

$$\phi(r) = \begin{cases} \frac{1}{8} \left(3 - 2r - \sqrt{1 + 4r - 4r^2} \right), & |r| < 1 \\ \frac{1}{8} \left(5 - 2r - \sqrt{-7 + 12r - 4r^2} \right), & 1 < |r| < 2 \\ 0, & \text{otherwise.} \end{cases}$$

5.2. Numerical examples.

Example 5.1. A free particle model for a Gaussian pulse: $V(x) = 0$. The initial data is taken to be $f(0, x, \xi) = \rho_0(x)\delta(\xi - u_0(x))$, where $\rho_0(x) = \exp(-(x - 0.5)^2)$, and $u_0(x) = -\sin(\pi x)|\sin(\pi x)|$. This example is taken from [10]. We plot the solutions at time $t = 1$, “OUR” indicates the numerical solution obtained by our method, “AVE/CONV/RED” indicates the numerical solutions obtained by the “AVE/CONV/RED” recovery procedures. In these four methods, the time step is taken to be $\Delta t = \Delta x/5$, where $\Delta x = 2/N$, N is the number of particles.

We show the multi-valued solutions \tilde{u} and $\tilde{\rho}$ at time $t = 1$ obtained by our method with $N = 400$ in Figure 1. One can compare them with Figures 7, 8 and 9 in [10] which are numerical solutions of this problem obtained by the moment methods, and our method yields much better numerical solutions.

We also compare our result with solutions obtained by previous particle methods. One can see in Fig 2, that the solutions obtained by AVE and RED methods are oscillatory. Fig 2 also shows that our solution is much better than the CONV solution, especially around the caustics. Fig 3 shows the comparison between our solution and exact solution which is obtained by taking Δx and Δt very small. One can see that they match very well.

When using the CONV method, one has to choose the width of the Gaussian kernel. We show solutions for different choices of the width in Fig 4. One can see that for large width δ , the solution is severely smeared, while for small δ , the solution becomes oscillatory. The best choice turns out to be 0.004 for this example. No formula has been given on how to choose δ

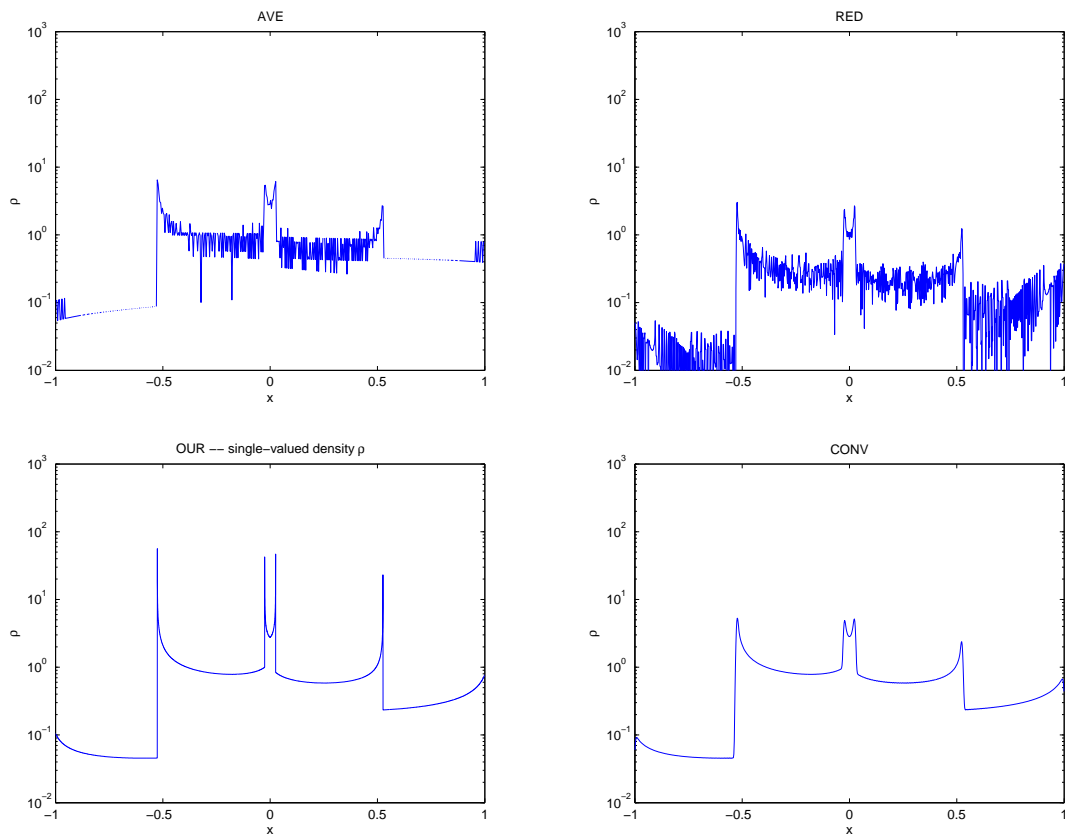


Figure 2: Example 5.1, single-valued density ρ with 1000 particles, $t=1$. Upper left: AVE, upper right: RED, lower left: OUR, lower right: CONV.

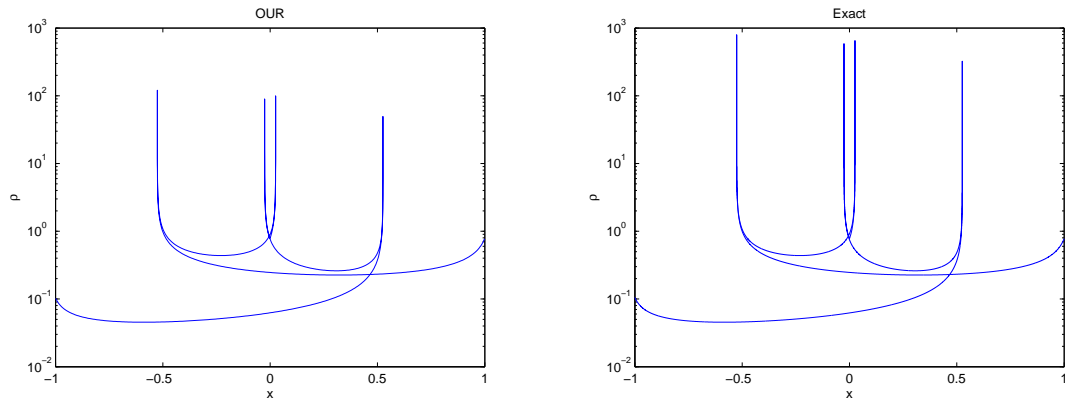


Figure 3: Example 5.1, multi-valued density $\tilde{\rho}$ at $t=1$, left: OUR with 1000 particles, right: Exact solution, $t=1$.

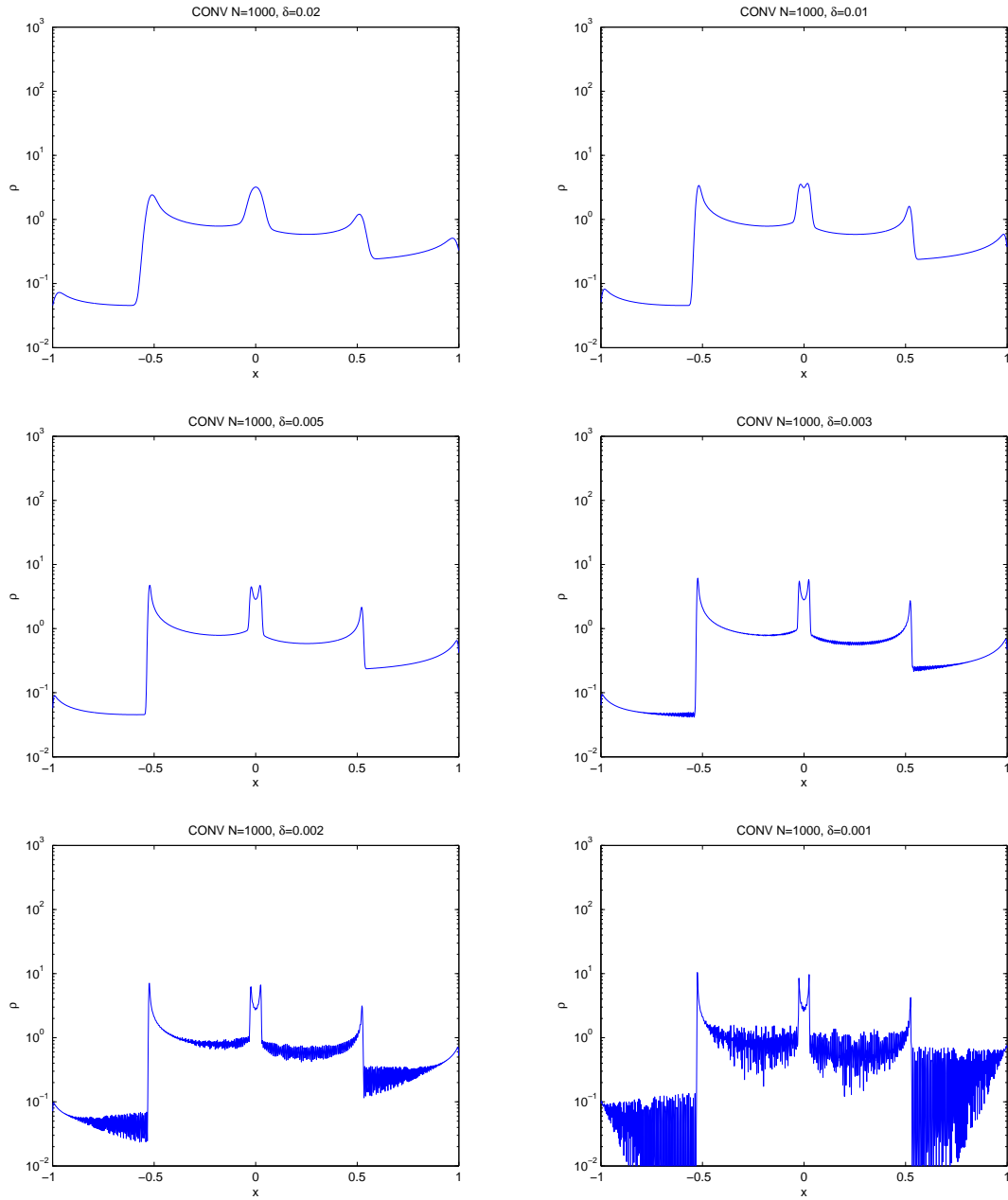


Figure 4: Example 5.1, density ρ obtained by CONV with 1000 particles at $t=1$ with different δ .

for general problems. Our solution outperforms the CONV method even with the best choice $\delta = 0.004$.

Example 5.2. In this example (taken from [4], example 4.3), the initial data are given by $f(0, x, \xi) = \rho_0(x)\delta(\xi - u_0(x))$, where $\rho_0(x) = 1$, $u_0(x) = 1 - 0.5 \arctan(20x)$, and the potential is $V(x) \equiv 0$. We compute the solution with $N = 400$ and output the solution at $t = 0.4$. In [4]

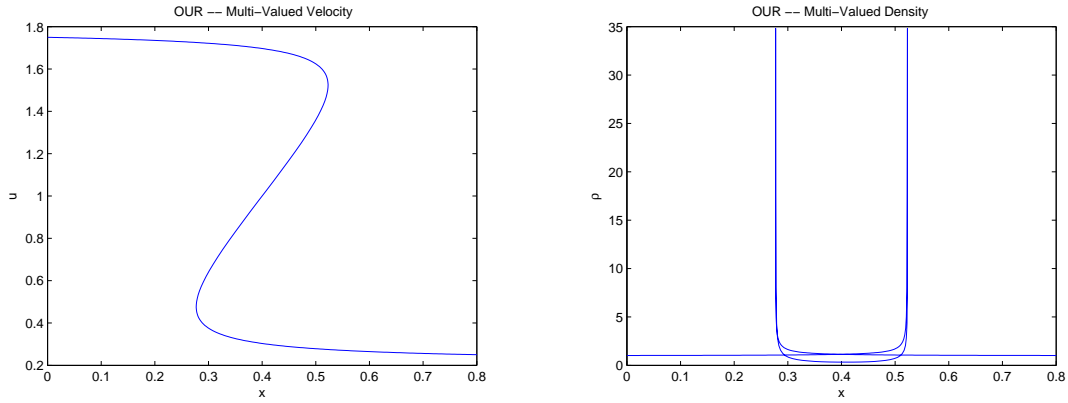


Figure 5: Example 5.2, left: multi-valued velocity \tilde{u} , right: multi-valued density $\tilde{\rho}$, $t=0.4$.

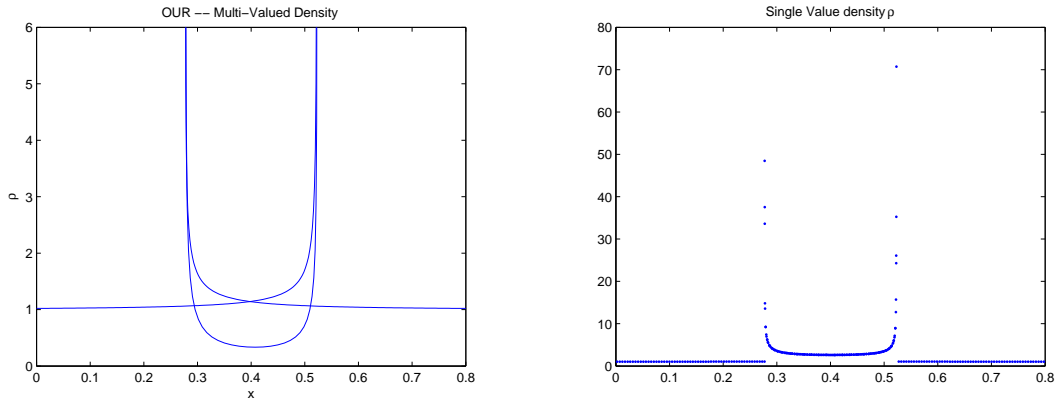


Figure 6: Example 5.2, left: multi-valued density $\tilde{\rho}$ zoomin, right: single-valued density ρ , $t=0.4$.

AVE, RED and CONV particle methods had been performed with the same particle number $N = 400$ (figures 5 and 6, page 574). The AVE and RED solutions are very oscillatory, while the CONV method with the best choice of $\delta = 0.1\sqrt{0.005}$ yields a better solution but still has oscillation. If one doubles δ , then it is oscillation-free, but the peaks in the density are much lower, i.e., peaks equal 5 for bigger δ and 6 for smaller δ . Our method yields much better results: our solutions are oscillation-free, much more accurate at peaks – the peak value of our solution is around 70. See Figures 5 and 6.

The following examples are numerical solutions of the Vlasov-Poisson equations. We compare our method with the CONV particle method. The main difference of the two methods is: in our method, we use (3.6) and (3.10) to calculate the local density ρ on *uniform mesh points* in each time step, then solve the Poisson equation; in CONV, we use (5.5) to calculate the local density ρ on *uniform mesh points* in each time step.

Example 5.3. We solve the 1D Vlasov-Poisson equations with periodic initial data

$$\begin{aligned} \frac{\partial f}{\partial t} + v \frac{\partial f}{\partial x} - E(x, t) \frac{\partial f}{\partial v} &= 0, \\ \frac{\partial^2}{\partial x^2} V &= \int_{-\infty}^{\infty} f(x, v, t) dv - 1, \quad E = -\frac{\partial V}{\partial x}, \\ f_0 &= \delta(v - \sin(2\pi x)). \end{aligned}$$

We compare density ρ , and electric field E obtained by different methods with different particle numbers N at $t = 0.5$. When solving the Poisson equation, we take the boundary condition $\phi(0) = \phi(1) = 0$. We take $\Delta t = \Delta x = 1/N$. The results are shown in Figs 7, 8.

One can see that our method yields much better solutions for the density ρ and electric field E . Furthermore, when apply the CONV method, for each N , we do serval tests for different widths of the Gaussian kernel δ , and show the best in our graphs. Hence, our method out performs the best that a CONV method can do, especially when N is small.

Example 5.4. We solve the 2D Vlasov-Poisson equation

$$\begin{aligned} f_t + \mathbf{v} \cdot \nabla_{\mathbf{x}} f - \mathbf{E}(\mathbf{x}, t) \cdot \nabla_{\mathbf{v}} f &= 0, \\ \Delta_{\mathbf{x}} V &= \int_{\mathbb{R}^2} f(\mathbf{x}, \mathbf{v}, t) dv, \quad E = -\nabla_{\mathbf{x}} V, \end{aligned} \tag{5.6}$$

with initial data

$$f(0, \mathbf{x}, \boldsymbol{\xi}) = \rho_0(\mathbf{x}) \delta(\boldsymbol{\xi} - \mathbf{u}_0(\mathbf{x})),$$

where

$$\rho_0 = I_{|\mathbf{x} - (1,1)| < 0.75}, \quad \mathbf{u}_0 = \frac{2 \sin \left(4\pi \left| \frac{4}{3}(\mathbf{x} - (1,1)) \right|^{5/6} \right) (\mathbf{x} - (1,1))}{3 \left| \mathbf{x} - (1,1) \right|}.$$

We calculate the solution on spatial domain $[0, 2] \times [0, 2]$. The initial particles are placed on $[-0.75, 0.75] \times [-0.75, 0.75]$, with $\Delta x = \Delta y = 1.5/N$. The uniform meshes for the Poisson equation are on domain $[0, 2] \times [0, 2]$ with $\Delta x = \Delta y = 2/N$. Δt is chosen to be $1/2N$. When solving the Poisson equation, we take the following boundary condition

$$\phi(0, \cdot) = \phi(2, \cdot) = \phi(\cdot, 0) = \phi(\cdot, 2) = 0.$$

The initial velocity profile is shown in Fig 9. For short times, if one ignores the Poisson potential, one can still gain some information (such like the basic shape) of the velocity profile. The velocity at $t = 0.2$ without involving the Poisson potential is shown in Fig 9, which suggests that for the Vlasov-Poisson equations of this example four caustics will form at $t = 0.2$.

We compare the density ρ and potential V obtained by our method and the CONV particle method with different N at $t = 0.2$. The results are shown in Figs 10, 11, and 12. The time cost for each method with different N are listed in Table 1. Roughly speaking, with the same particle number, the time cost of the new method is approximately 1/10 of the CONV particle method. The largest local density near the caustics that obtained by the new method and the CONV particle method are listed in Table 2. Combine these results, we can say that compared

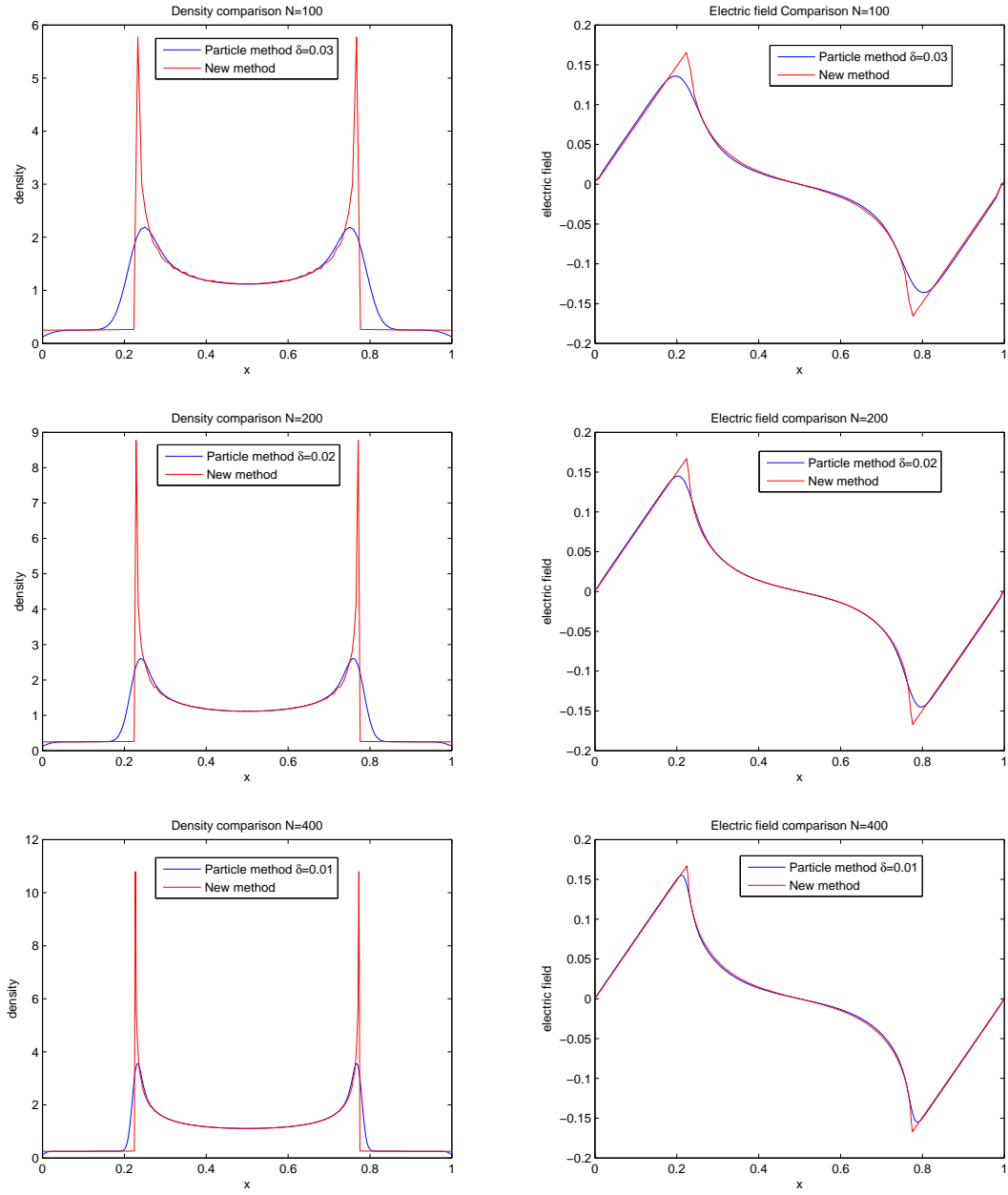


Figure 7: Example 5.3, left: density ρ , right: electric field E .

with the CONV particle method our new method yields better numerical results with less computational cost.

6. CONCLUDING REMARKS

In this paper, we proposed a new numerical method for the semiclassical limit of the Schrödinger equation (the Liouville equation with measure-valued initial data) and Vlasov-Poisson equations. Our method constructs local density based on a conservative quantity—the charge. Therefore

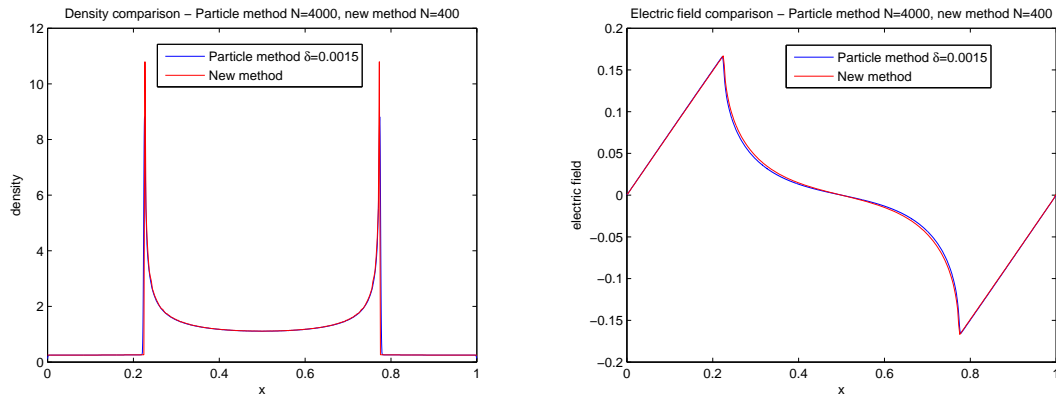


Figure 8: Example 5.3, comparison between OUR with $N=400$ and CONV with $N=4000$, left: density ρ , right: electric field E .

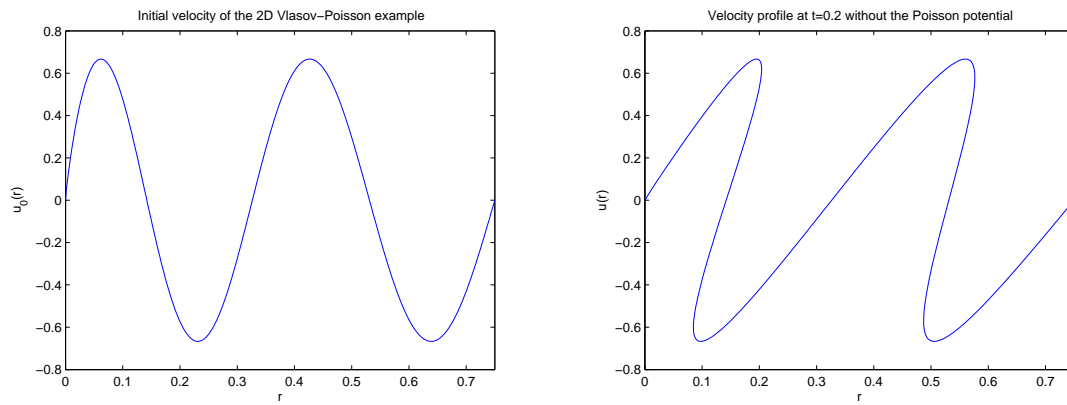


Figure 9: Example 5.4, left: initial velocity, right: velocity at $t=0.2$ without the Poisson potential.

	$N = 50$	$N = 100$	$N = 150$	$N = 200$	
New method	40	807		17493	(seconds)
CONV method	435	10735	113318		(seconds)

TABLE 1. Example 5.4, comparison of the time cost of the new method and the CONV particle method.

it avoids the smoothing procedures of the previous particle methods. Numerical examples verify that compared with the previous particle methods our method yields better numerical solutions with less computational cost.

	$N = 50$	$N = 100$	$N = 150$	$N = 200$
New method: $\max \rho$	12.6083	21.3102		80.3682
CONV method: $\max \rho$	1.9091	2.3927	2.9320	

TABLE 2. Example 5.4, comparison of $\max \rho$ of the new method and the CONV particle method.

REFERENCES

- [1] C.K. Birdsall, A.B. Langdon, Plasma Physics via Computer Simulation, Adam Hilger, New York, 1991.
- [2] F. Bouchut, Global weak solution of the Vlasov-Poisson system for small electrons mass, Comm PDEs, 16, 1337-1365, 1991.
- [3] L.-T. Cheng, H.-L. Liu and S. Osher, Computational high-frequency wave propagation using the Level Set method, with applications to the semi-classical limit of Schrödinger equations, Comm. Math. Sci. 1, 593-621, 2003.
- [4] A. Chertock and A. Kurganov, Computing Multivalued solutions of pressureless gas dynamics by deterministic particle methods, Commun. Comput. Phys. no. 2-4, 565-581, 2009.
- [5] A.J. Chorin, Numerical study of slightly viscous flow, J. FluidMech. 57, no. 4, 785-796, 1973.
- [6] G.-H. Cottet and P.D. Koumoutsakos, Vortex Methods, Cambridge University Press, Cambridge, 2000.
- [7] B. Engquist and O. Runborg, Computational high frequency wave propagation, Acta Numer. 12, 181-266, 2003.
- [8] F. Filbet, E. Sonnendreker, P. Bertrand, Conservative numerical schemes for the Vlasov equation, Journal of Computational Physics, 172, 166-187, 2001.
- [9] P. Gerard, P.A. Markowich, N.J. Mauser, and F. Poupaud. Homogenization limits and Wigner transforms, Comm. Pure Appl. Math., 50(4), 323-379, 1997.
- [10] L. Gosse, S. Jin and X. Li, On two moment systems for computing multiphase semiclassical limits of the Schrödinger equation, Math. Model Mech. Appl. Sci. 13, 1689-1723, 2003.
- [11] R. Hockney, J. Eastwood, Computer Simulation Using Particles, Institute of Physics Publishing, 1988.
- [12] S. Jin and X.T. Li, Multi-phase computations of the semiclassical limit of the Schrödinger equation and related problems: Whitham vs Wigner, Physica D, 182, 46-85, 2003.
- [13] S. Jin, P.A. Markowich and C. Sparber, Mathematical and computational methods for semiclassical Schrödinger equations, Acta Numerica, 2011, to appear.
- [14] S. Jin, H.L. Liu, S. Osher and R. Tsai, Computing multi-valued physical observables for high frequency limit of symmetric hyperbolic systems, J. Comp. Phys. 210, 497-518, 2005.
- [15] S. Jin and K. Novak, A Semiclassical Transport Model for Thin Quantum Barriers, Multiscale Modeling and Simulation, 5(4), 1063-1086, 2006.
- [16] S. Jin and K. Novak, A Semiclassical Transport Model for Two-Dimensional Thin Quantum Barriers, J. Comp. Phys. 226, 1623-1644, 2007.
- [17] S. Jin and S. Osher, A level set method for the computation of multi-valued solutions to quasi-linear hyperbolic PDE's and Hamilton-Jacobi equations, Comm. Math. Sci. 1(3), 575-591, 2003.
- [18] N.A. Krall and A.W. Trivelpiece, Principles of Plasma Physics, San Francisco Press, 1996.
- [19] P.L. Lions and T. Paul, Sur les mesures de Wigner, Revista. Mat. Iberoamericana 9, 553-618, 1993.
- [20] P.L. Lions and B. Perthame, Propagation of moments and regularity for the 3-dimensional Vlasov-Poisson system, Inventiones Mathematicae, 105, 415-430, 1991.
- [21] A. Majda, G. Majda and Y.X. Zheng, Concentrations in the one-dimensional Vlasov-Poisson equation I: Temporal development and non-unique weak solutions in the single component case, Physica D, 74, 268-300, 1994.

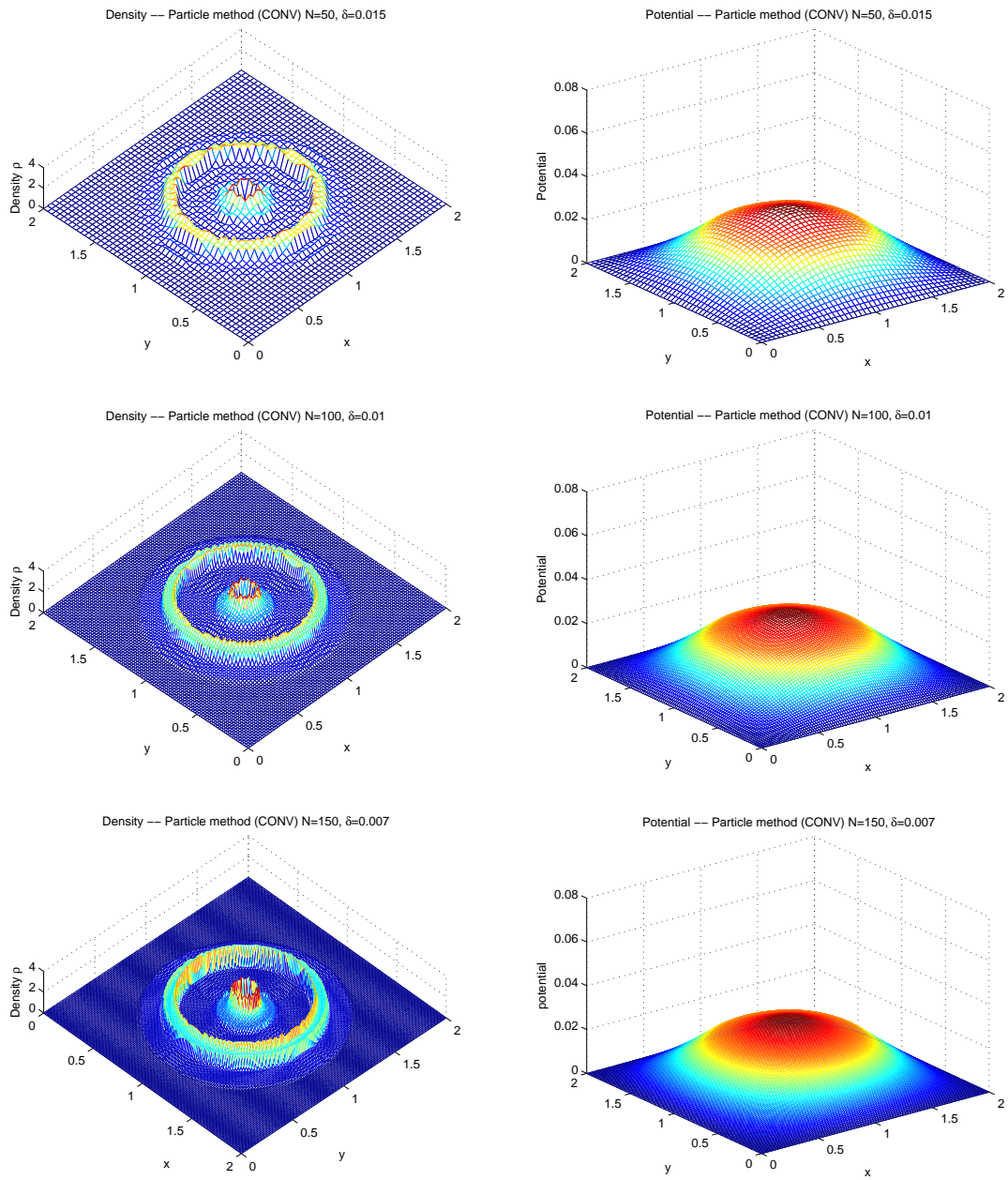
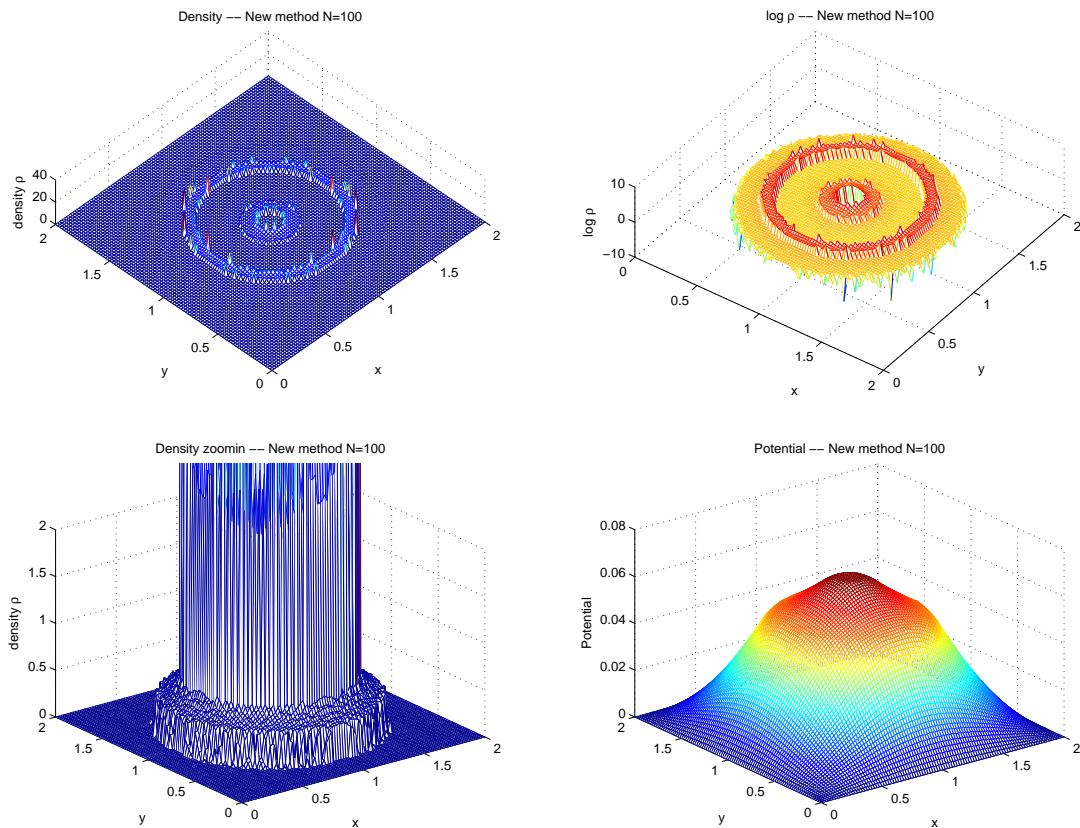


Figure 10: Example 5.4, the CONV particle method with different N and $\delta = 0.015$, left: density ρ , right: potential ϕ .

- [22] A. Majda, G. Majda and Y.X. Zheng, Concentrations in the one-dimensional Vlasov-Poisson equations. II: Screening and the necessity for measure-valued solutions in the two component case, *Physica D*, 79, 41-76, 1994.
- [23] P.A. Markowich and C.A. Ringhofer, *Semiconductor Equations*, Springer, 1990.
- [24] S. Osher, L.-T. Cheng, M. Kang, H. Shim and Y.-H. Tsai, Geometric optics in a phase-space-based level set and Eulerian framework, *J. Comput. Phys.* 179(2), 622-648, 2002.

Figure 11: Example 5.4, New method, $N=100$.

- [25] C.S. Peskin, The immersed boundary method, *Acta Numer.* 11, 479-517, 2002.
- [26] P.-A. Raviart, An analysis of particle methods, *Numerical methods in fluid dynamics (Como, 1983)*, Lecture Notes in Math., vol. 1127, Springer, Berlin, 243324, 1985.
- [27] C. Sparber, P. Markowich and N. Mauser, Wigner functions versus WKB methods in multivalued geometrical optics, *Asymptot. Anal.* 33(2), 153-187, 2003.
- [28] J. Vay, P. Colella, P. Mccorquodale, B. Van Straalen, A. Friedman, D. Grote, Mesh refinement for particle-in-cell plasma simulations: applications to and benefits for heavy ion fusion, *Laser and Particle Beams*, 20, 569575, 2003.
- [29] J. Verboncoeur, Particle simulation of plasmas: review and advances, *Plasma Physics and Controlled Fusion*, 47 (2005) 46.
- [30] D. Wei, 1D Vlasov-Poisson equations with electron sheet initial data, *Kinetic and Related Models*, Volume 3, Number 4, 729-754, 2010, doi:10.3934/krm.2010.3.729.
- [31] Y.X. Zheng and A. Majda, *Existence of global weak solutions to one-component Vlasov-Poisson and Fokker-Planck-Poisson systems in one space dimension with measures as initial data*, *Comm. on Pure and Applied Math.* Vol. XLVII, 1365-1401, 1994.

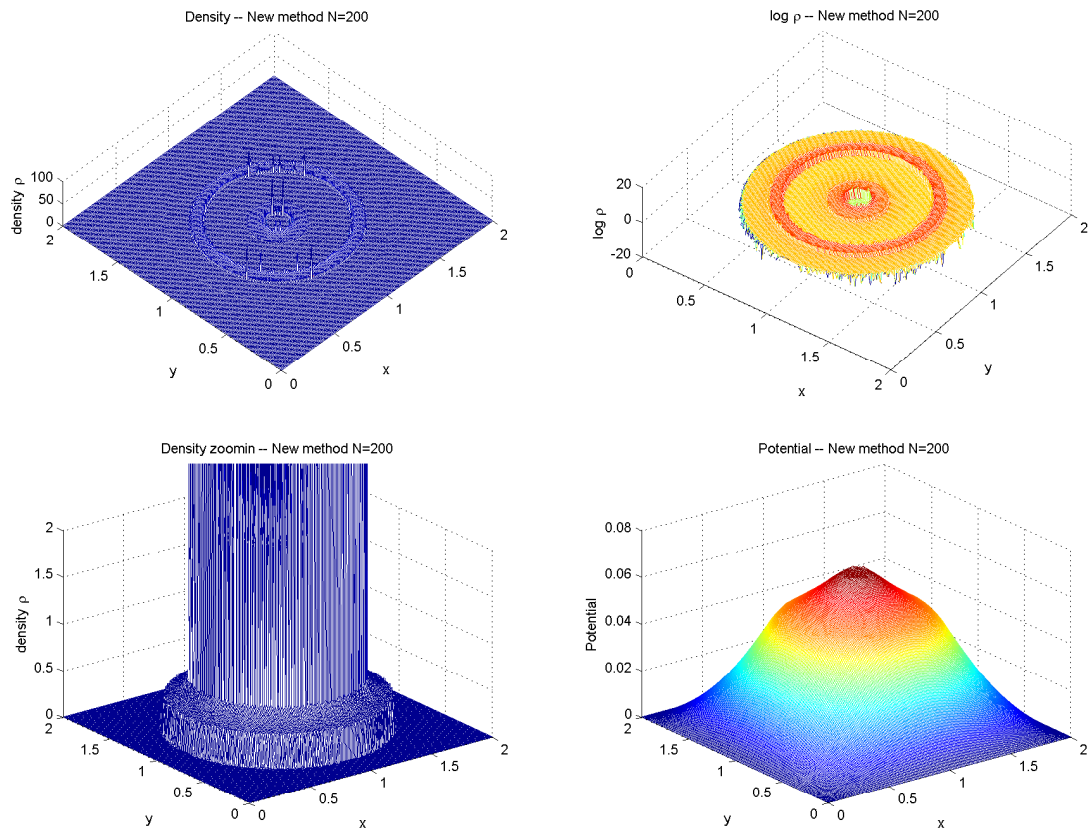


Figure 12: Example 5.4, New method, N=200.

(Shi Jin)

DEPARTMENT OF MATHEMATICS

UNIVERSITY OF WISCONSIN

MADISON, WI 53706 USA

E-mail address: jin@math.wisc.edu

(Dongming Wei)

DEPARTMENT OF MATHEMATICS

UNIVERSITY OF WISCONSIN

MADISON, WI 53706 USA

E-mail address: dwei@math.wisc.edu